Forside

Eksamensinformation
NFYK10020E - Physics Thesis 60 ECTS, Niels Bohr Institute - Kontrakt:140666 (Yan Yu)

Besvarelsen afleveres af
Yan Yu
nzw726@alumni.ku.dk

Eksamensadministratorer
Eksamensteam, tel 35 33 64 57
eksamen@science.ku.dk

Bedømmere
Johan Georg Mulvad Samsing
Eksaminator
jsamsing@nbi.ku.dk
+4535320370

Marta Orselli
Censor
orselli@nbi.ku.dk

Besvarelsesinformationer

Titel: Gravitational Lensing Effect in Triple Black Hole System
Titel, engelsk: Gravitational Lensing Effect in Triple Black Hole System
Tro og love-erklæring: Ja
Indeholder besvarelsen fortroligt materiale: Ja

UNIVERSITY OF COPENHAGEN

Master Dissertation in Astrophysics

Gravitational Lensing Effect in Triple Black Hole System

Yan Yu

Niels Bohr International Academy

Supervisor: Johan Samsing and Troels Harmark

May 2024

ACKNOWLEDGEMENTS

I would like to thank my supervisor Johan Samsing and co-supervisor Troels Harmark. I appreciate Johan's unwavering guidance and support as well as Troels' invaluable advice throughout this research journey. It was their enthusiasm, seriousness, creativity, and insightful discussions in Astrophysics that impressed me deeply and encouraged my life ideal of continuing to do research and explore the Universe.

I am also very grateful to the people working at NBI, including professors Martin and Daniel, as well as Gaia, Kai, David, Lorenz, Alessandro, and Edgar. As an international student studying abroad for the first time, I would not have been able to adapt to the environment quickly without their help. The several discussions they had with me also benefited me a lot.

I am also very grateful for the support from my parents Hong and Shaohai, and my boyfriend Shaowen. Even though my parents and I are separated by an ocean, their tolerance, support, and expectations are the foundation for me to overcome all difficulties. My boyfriend and I have the same life ideals, we always encourage each other. His laughter always pulled me out of depression.

I loved my time studying at Niels Bohr Institute in the University of Copenhagen and am sincerely grateful to everyone I met here. It is the people and things here that continue to broaden my horizons and exercise my abilities, allowing me to gain the confidence and ability to face all opportunities and challenges in the future. I sincerely wish everyone will get better and better.

ABSTRACT

The origin of the binary black hole is one of the most charming, cutting-edge, and active Astrophysical topics. One of the possible formation channels is dynamical formation under the effect of another compact object, during which there must exist a triple system. In order to test the existence of the third object, we focus on the gravitational lensing effect on the Gravitational Waves emitted from the binary system. When we consider the binary as the gravitational source and the third object as the lens, the amplification factor which is a function of both frequency and position will show differences under different source parameter combinations and orbital types when the source is inside the defined obvious lensing window, which will help us infer the source information and separate different orbits. In this work, we mainly focus on the magnification difference between circular and straight orbits with different incoming directions under low-velocity conditions.

CONTENTS

LIST OF FIGURES

Part I

INTRODUCTION

1

INTRODUCTION

One of the most cutting-edge unsolved astrophysical problems is the origin of the binary black hole (BBH), especially the eccentric binary black holes. According to the previous research work, one possible formation channel is under the influence of another black hole (*Rodriguez, Amaro-Seoane, et al. 2018*), which means there exists a time period during which the three Black Holes (BHs) form a triple system, either hierarchical bound or under chaotic resonance. In order to find whether a binary is formed through this channel, we use Gravitational Wave (GW) as our probe to infer the source information.

The environmental perturbation on the gravitational wave emitted from the binary can be divided into two main classes: one is gaseous friction and the other is from the gravitational field of the tertiary black hole. The latter case contains three more specific effects: gravitational lensing effect, Doppler effect and Newtonian tidal effect(*Yu et al. 2021*). In this work, we will first review some previous research work and then try to find whether it is reasonable to infer the orbital type and source parameters only from the gravitational lensing effect, in which the binary is considered as the gravitational-wave source and the tertiary black hole as the lens.

We will concentrate on the simplest moving case: both inner and outer orbits are circular. The inner orbit is defined as the orbit inside the BBH and the outer orbit as the trajectory of the binary center-of-mass(COM). The most significant parameter we use is the amplification factor F in a moving system, which is a function of both GW frequency and source position parameters. By combining the evolution of inner BBH and outer orbit motion, we can calculate the magnification factor for any moving case inside the defined obvious lensing window. Different mass combinations, angular diameter distance combinations, orbit types and incoming directions will lead to magnification differences. Therefore, it is reasonable to infer the source information and outer orbit type only from the gravitational lensing effect.

Part II

BACKGROUND

2

GRAVITATIONAL WAVES

Gravitational Wave (GW) is the transverse wave solution of the linearized weak-field equation in General Relativity, which travels at the speed of light and possesses two polarizations. The brief derivation of the GW is shown in the following parts according to the *General Relativity and Cosmology Lecture Notes by Troels Harmark*:

In General Relativity, if we choose the weak field limit, the gravitational field is weak and the metric $g_{\mu\nu}(x)$ is approximately that of Minkowski space, which is written as:

$$g_{\mu\nu}(x) = \eta_{\mu\nu} + h_{\mu\nu}(x), \left|h_{\mu\nu}(x)\right| << 1 \tag{1}$$

Then if we expand the General Relativity to the first order in $h_{\mu\nu}(x)$, the weak field limit of the geodesic equation is Eq.2, which is also called the linearized geodesic equation:

$$\frac{d^2x^\rho}{d\tau^2} = -(\partial_\mu h_\nu^\rho - \frac{1}{2}\partial^\rho h_{\mu\nu})\frac{dx^\mu}{d\tau}\frac{dx^\nu}{d\tau} \tag{2}$$

The weak field limit of the Ricci tensor is calculated as:

$$R_{\mu\nu} = \frac{1}{2}(\partial_\mu\partial_\rho h_\nu^\rho + \partial_\nu\partial_\rho h_\mu^\rho - \Box h_{\mu\nu} - \partial_\mu\partial_\nu h_\rho^\rho) \tag{3}$$

Here the d'Alembert operator is:

$$\Box = \eta^{\mu\nu}\partial_\mu\partial_\nu = \partial_\mu\partial^\mu \tag{4}$$

If we combine the Eq.3 with Einstein equation Eq.5, linearized gravity will be got.

$$R_{\mu\nu} - \frac{1}{2}g_{\mu\nu}R = 8\pi G T_{\mu\nu} \tag{5}$$

In order to simplify the equations, we use the gauge transformation of $h_{\mu\nu}$ and choose Lorenz gauge, which is shown in Eq.6 and 7 respectively, where $\epsilon_\mu(x) = \eta_{\mu\nu}\epsilon^\nu(x)$.

$$\tilde{h_{\mu\nu}}(x) = h_{\mu\nu}(x) + \partial_\mu\epsilon_\nu(x) + \partial_\nu\epsilon_\mu(x) \tag{6}$$

$$\partial^\mu(h_{\mu\nu} - \frac{1}{2}\eta_{\mu\nu}h^\rho_\rho) = 0 \tag{7}$$

Combining Eq.7 and Eq.3 gives the weak field limit Ricci tensor in Lorenz Gauge:

$$R_{\mu\nu} = -\frac{1}{2}\Box h_{\mu\nu} \tag{8}$$

which subsequently leads to the linearized Einstein equations:

$$\Box h_{\mu\nu} = -16\pi G(T_{\mu\nu} - \frac{1}{2}\eta_{\mu\nu}\eta^{\rho\sigma}T_{\rho\sigma}) \tag{9}$$

In vacuum case $T_{\mu\nu} = 0$:

$$\Box h_{\mu\nu} = 0 \tag{10}$$

Eventually, the wave solution which is considered as the gravitational wave:

$$h_{\mu\nu} = Re[A_{\mu\nu}exp(ik_\rho x^\rho)] \tag{11}$$

$$k^\mu = (\omega, k^1, k^2, k^3), k^\mu k_\mu = 0 \tag{12}$$

When it comes to the observation, a generic test is used which means comparing the observed signals with theoretically predicted waveform to get information about the source. The detector principle is to measure the variations of the light travel time between separated test masses, which is caused by the GW passing(*Bailes et al. 2021*). Detectors can be categorized into two types, ground-based detectors such as LIGO, and space-based detectors including LISA.

Gravitational Wave has many important applications. First, it can provide unique messages of the most energetic astrophysical process by carrying dynamical information of massive objects such as Binary Black Hole moving at relativistic speeds. Second, it has the potential to answer the fundamental questions including the formation and evolution of Binary Black Holes (BBH) as well as the origin of dark matter and dark energy (*Bailes et al. 2021*).

3

BINARY BLACK HOLE AND CORRESPONDING GW

3.1 BBH FORMATION CHANNEL

Binary Black Hole (BBH) is considered one of the most important sources for Gravitational Waves (GW). However, more research is still needed to unveil the mystery of BBH formation channel details. Previous work has already unveiled most of the formation channels fall into the following 2 types (*Rodriguez, Amaro-Seoane, et al. 2018*): BBH is the remnant of isolated massive binary stars, or BBH is the result of dynamical interactions in a dense stellar environment. The two different types of formation may happen at the same time in actual formation and evolution, so it is a challenge to extract very detailed information for certain cases.

The product of both formation types are able to generate BBH with certain mass, spin, and merger rates and corresponding GW inside the detector band such as LIGO (*Amaro-Seoane and Chen 2016*). One of the most significant differences between the two formation channels is the binary eccentricity. For the BBH as a remnant of massive binary stars, GW emission will efficiently circularize the orbit long before the GW signal enters the current detector band. However, in the dynamical formation channel, eccentric orbits can be realized either through the influence of a third object or from the direct dynamical interaction under Post-Newtonian approximation.

When we focus on the dynamical channel, there will be some probabilities for the BBH to merge in dense environments such as Globular Clusters (GC), and the induction factors will be different. According to the factors leading to the final merger, the BBH can be divided into the following four types (*Rodriguez, Amaro-Seoane, et al. 2018*): a) Primordial binaries: Occurs in the isolated binaries and never encounters a strong dynamical interaction. b) Ejected mergers (*Rodriguez, Chatterjee, et al. 2016*): Binary will encounter many encounters before it is ejected from the initial environment and finally merges outside. c) In-cluster mergers: binary merge inside the initial clusters after some encounters but not due to the GW emission. d) GW captures: binary merge after a close encounter, to be more specific, merge through resonant encounters as a result of GW emission.

The encounters mentioned above mean the event when a binary meets another object in the surrounding environment and either interacts with or is perturbed by it. When it comes to the binary-single encounters, it can be divided into several different categories depending on the initial conditions as well as the final outcomes, which is shown in Fig.1.

Weak Perturbation (WP) refers to the case binary is only perturbed by another single object over several orbital periods. Strong Perturbation (SP) occurs when the third object follows a hyperbolic trajectory around the binary at a distance close to the binary SMA (*Heggie 1975*). A Close Interaction (CI) occurs when the third object is inside the influence sphere $r_{CI} = \frac{m_2}{m_1+m_2}a_0, m_2 > m_1$. m_1, m_2 are the masses of the binary components. CI contains two cases, which are the Resonance Interaction (RI) and Direct Interaction (DI).

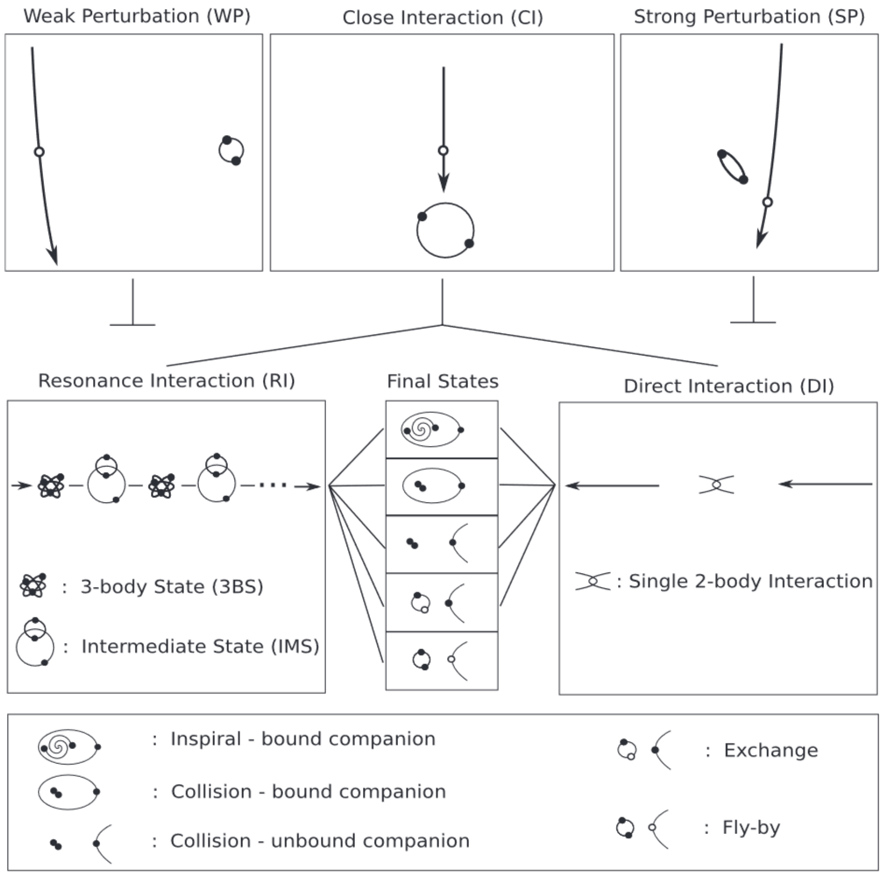

Figure 1: Schematic figure to show binary-single interaction and their final states in *Samsing et al. 2014*.

3.2 BBH EVOLUTION: PETER'S EQUATION

The evolution of the BBH, especially the final stages can be divided mainly into three types: the inspiral, the merger, and the ringdown of the remnant black hole (*Schmidt 2020*). Here we mainly focus on the inspiral and merger stage, as well as the corresponding GW.

According to *Philip Carl Peters 1964*, the evolution of an eccentric BBH can be described by component masses, semi-major-axis (SMA) a and the eccentricity e:

$$\langle\frac{da}{dt}\rangle = -\frac{64}{5}\frac{G^3 m_1 m_2 (m_1+m_2)}{c^5 a^3 (1-e^2)^{7/2}}(1+\frac{73}{24}e^2+\frac{37}{96}e^4) \tag{13}$$

$$\langle\frac{de}{dt}\rangle = -\frac{304}{15}e\frac{G^3 m_1 m_2 (m_1+m_2)}{c^5 a^4 (1-e^2)^{5/2}}(1+\frac{121}{304}e^2) \tag{14}$$

If we concentrate on the Keplerian orbits:

$$a^3 = P^2\frac{G(M_1+M_2)}{4\pi^2} \tag{15}$$

Insert the Eq.15 into Eq.13 and 14, we will also get:

$$\langle\frac{dP}{dt}\rangle = -\frac{192\pi}{5c^5}(\frac{2\pi G}{P})^{5/3}\frac{m_1 m_2}{(m_1+m_2)^{1/3}}\frac{1+\frac{73}{24}e^2+\frac{37}{96}e^4}{(1-e^2)^{7/2}} \tag{16}$$

$$\langle\frac{de}{dt}\rangle = -\frac{608\pi}{15c^5}\frac{e}{P}(\frac{2\pi G}{P})^{5/3}\frac{m_1 m_2}{(m_1+m_2)^{1/3}}\frac{1+\frac{121}{304}e^2}{(1-e^2)^{5/2}} \tag{17}$$

The evolution equations above also describe how the SMA changes with eccentricity by a differential equation by combining Eq.13 and 14:

$$a(e) = c_0\frac{e^{12/19}}{1-e^2}[1+\frac{121}{304}e^2]^{870/2299} \tag{18}$$

Here c_0 depends on the initial conditions (m_1, m_2, a_0, e_0) of the BBH. Fig.2 is a reconstruction of the figure shown in *Philip Carl Peters 1964*, which describes how the SMA changes with e.

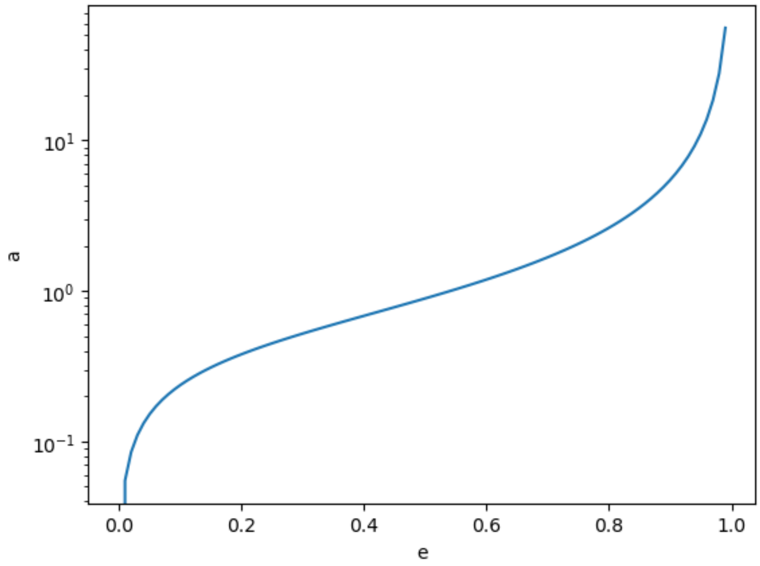

Figure 2: Semi-major-axis a as a function of eccentricity e.

Once we get the evolution of a and e, the dominant frequency of the GW radiated by the BBH at each time point can be calculated approximately as Eq.53 (*Philip C Peters and Mathews 1963, Philip Carl Peters 1964, Rodriguez, Amaro-Seoane, et al. 2018, Wen 2003*), in which M is the total mass of the source binary:

$$f_{GW} = \frac{\sqrt{GM}}{\pi}\frac{(1+e)^{1.1954}}{[a(1-e^2)]^{3/2}} \tag{19}$$

In Fig.2, semi-major axis a changes rapidly near two endpoints, i.e. $e\sim 0$ and $e\sim 1$. $e\sim 0$ refers to the stage approaching to the merger. Since a decreases when the evolution goes towards the merger, the dominant frequency of the GW in Eq.53 will increase continuously until it reaches the merger point, leading to the chirp signal which is consistent with the observation.

3.3 GW FROM BBH

More than 10 BBHs have been identified through detection since the first landmark detection of GWs from the coalescence of two stellar-mass BHs in 2015 by the Advanced LIGO GW-detectors (*B. P. Abbott et al. 2016*, *Schmidt 2020*).

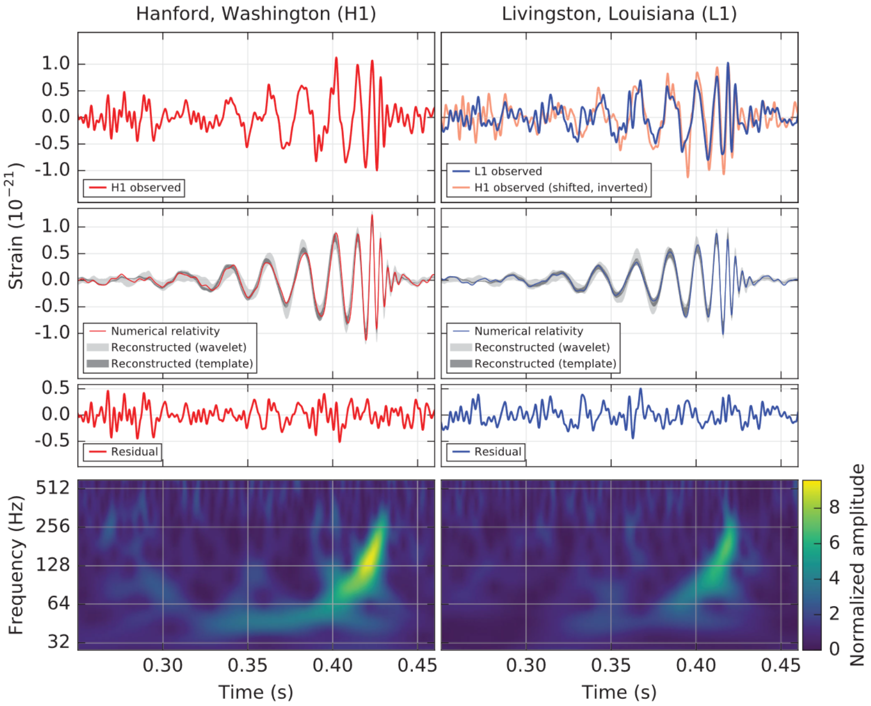

Figure 3: The direct observation results of GW150914, the binary black hole merger event in *B. P. Abbott et al. 2016*.

Fig.3 is the result of the first observation GW signal. All the time series in these subfigures are filtered in the frequency region [35,350] Hz, in order to decrease the influence of the fluctuations outside the detector's most sensitive frequency band. The top row shows the signal strain detected by the two detectors. The second row refers to the comparison between waveforms from different construction methods. The bottom row shows the signal frequency continuously increases which is consistent with theoretical calculation result approximation Eq.53.

4

GRAVITATIONAL LENSING EFFECT

After Johann Soldner's first thinking and exploration of the light deflection by gravity using Newtonian physics, Einstein directly addressed the influence of gravity on the light in 1911 with the same results as Johann Soldner but it differs from the actual correct answer by a factor equal to 2, and finally derived the correct deflection angle of a light ray by using General Relativity: $\alpha = \frac{4GM}{c^2}\frac{1}{r}$, where M is the lens mass, c is the light speed and r is the distance between the incoming light ray and the object. In the following century, the gravitational lensing effect was found to be a very useful tool in astronomy and astrophysics due to its unique magnification property and different consequent multiple images. Gravitational lensing effect also occurs when it comes to the Gravitational Waves. Although unlike multiple images observed for the light bundle case, the lensed GW signals also show some magnification.

4.1 LENSING ON LIGHT

4.1.1 *Approximation*

When the light bundle is propagating through the universe, its path, size, and cross-section will be influenced by all the matter between it and the observer. In order to calculate the final lensing effect, some approximations are needed, including the underlying spacetime and several lens approximations.

For the underlying spacetime, we assume it can be described by the perturbed Friedmann-Robertson-Walker metric:

$$ds^2 = (1 + \frac{2\Phi}{c^2})c^2dt^2 - a^2(t)(1 - \frac{2\Phi}{c^2})d\sigma^2 \tag{20}$$

For the lens, we use both the thin lens approximation and the point-mass model. Thin lens approximation describes all the deflection action that takes place at a single distance, which is valid when $v << c$ and $|\Phi| << c^2$. Here v is the relative velocities of the source, lens, and observer, $|\Phi|$ is the Newtonian potential. (*Wambsganss 1998*)

4.1.2 *Lens Equation*

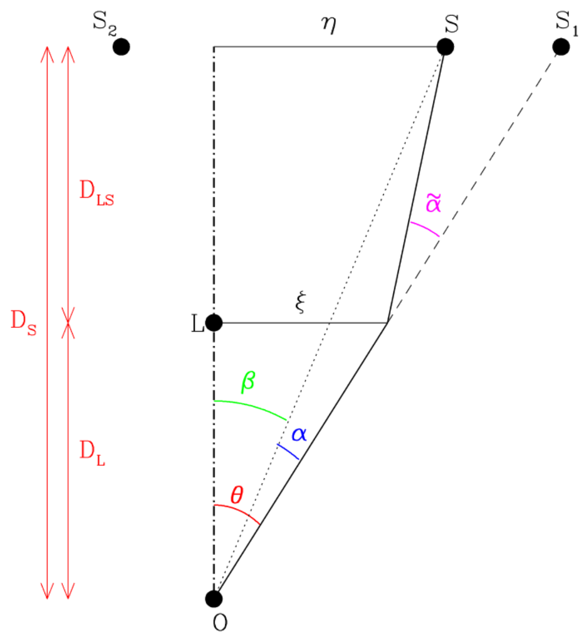

Figure 4: A simplified gravitational lens scenario in *Wambsganss 1998*. The source, lens, and observer are considered as points. θ and β are the angle positions of the image and source respectively.

Fig.4 shows a simplified gravitational lensing scenario for the simplest lensing case: the object L is a point-like lens, and the light emitted from the source S is deflected by the lens and consequently forms two images S_1 and S_2. θ is the angular position of image, β is the angular positon of the source, $\tilde{\alpha}$ is the deflection angle. In the circular-symmetric case, the deflection angle is:

$$\tilde{\alpha}(\xi) = \frac{4GM(\xi)}{c^2}\frac{1}{\xi} \tag{21}$$

Here $M(\xi)$ refers to the mass inside the region with radius ξ. D_L, D_S, D_{LS} are the relevant angular diameter distance between observer and lens, observer and source, lens and source respectively. If we consider the point-mass lens model, and the distance is so large that $\beta, \theta, \tilde{\alpha} << 1$, from the Fig.4 we can derive the lens equation in the following steps:

$$\theta D_S = \beta D_S + \tilde{\alpha} D_{LS} \tag{22}$$

$$\tilde{\alpha} D_{LS} = \alpha D_S \tag{23}$$

$$\beta = \theta - \alpha(\theta), \alpha(\theta) = \frac{D_{LS}}{D_S}\tilde{\alpha}(\theta) \tag{24}$$

4.1.3 *Einstein Radius*

By inserting the relation of $\xi = \theta D_L$ shown in Fig.4 into Lens Equation 24 we can obtain:

$$\beta(\theta) = \theta - \frac{D_{LS}}{D_L D_S}\frac{4GM}{c^2\theta} \tag{25}$$

One special case in the gravitational lensing effect is when the source is just behind the lens and forms a highly alignment case, described by $\beta = 0$. In this case, Eq.25 gives the special angle called the Einstein angle (also called Einstein radius in some previous work):

$$\theta_E = \sqrt{\frac{D_{LS}}{D_L D_S}\frac{4GM}{c^2}} \tag{26}$$

The characteristic image of this case is the Einstein Ring with a radius of $r_E = \theta_E D_S$.

If we transform the unit into the case for a triple BH system, the Einstein angle is:

$$\theta_E = (\frac{M_L}{10^{11.09}M_\odot})^{1/2}(\frac{D_L D_S/D_{LS}}{Gpc})^{-1/2} arcsec \tag{27}$$

4.2 LENSING ON GW

4.2.1 *Amplification Factor Calculation*

When it comes to the gravitational lensing effect on the GW, wave optics should be used due to its much longer wavelength, instead of the geometric optics for the light case. The difference between wave optics and geometric optics on the gravitational lensing results can be mainly divided into two kinds: wave effects and strong lensing region. Wave effects include diffraction and interference, and the strong lensing region refers to the source region leading to the obvious magnification.

In order to calculate the gravitational lensing effect in the case of BBH as the GW source and tertiary BH as the lens, Thin Lens Approximation and Point Mass Model are used. The geometric schematic figure of this case is shown in Fig.5. The lens here is the tertiary black hole, and the source is the COM of the binary. η is the position vector referring to the distance between the source and the lens projection position on the source plane. ξ is the impact parameter of the lens.

First let us talk about the wave effect, especially the diffraction. Since the GW has such a long wavelength, if the wavelength λ is much larger than the Schwarzchild radius of the lens object $r_S = \frac{2GM_L}{c^2}$ (the radius defining the event horizon of a Schwarzschild black hole), the diffraction will be large enough and make the magnification small. According to *T. T. Nakamura 1998*, if we consider a double slit with lens Einstein radius $\xi_E \sim (M_L D)^{1/2}$ as the slit width, where D is the distance between the observer and the slit, then the width of the central peak for the interference pattern is $\frac{D}{\xi_E}\lambda$, λ is the wavelength. As a result, the maximum magnification is of the order $\sim \frac{\xi_E}{(\frac{D}{\xi_E}\lambda)} \sim \frac{M_L}{\lambda}$. If we convert the units to the scale of the actual cases, the region for apparent diffraction effect is:

$$M_L \leq 10^8 M_{\odot} (\frac{f}{mHz})^{-1} \tag{28}$$

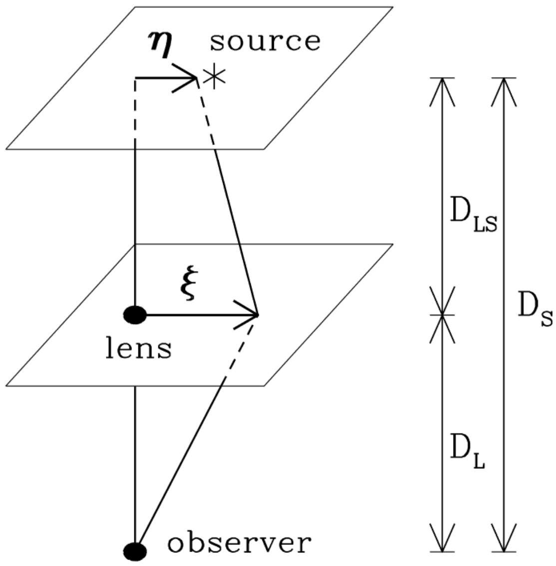

Figure 5: Gravitational lens geometry for the source, lens, and the observer. Here D_L,D_s, and D_{LS} refer to the distance between lens and observer, source and observer, lens and the source. The η is the position vector of the source in the source plane, and ξ is the impact parameter of the lens (the closest approach).

Second let us calculate the magnification factor, which is the most important step to get a lensed GW signal since the lensed signal is the product of the magnification factor and unlensed signal:

$$h^{\tilde{L}}_{+,\times}(f) = F(f)h^{\tilde{}}_{+,\times} \tag{29}$$

According to *Takahashi and T. Nakamura* 2003, the amplification factor in the Fig.5 case is:

$$F(f) = exp\{\frac{\pi\omega}{4} + i\frac{\omega}{2}[ln(\frac{\omega}{2}) - 2\phi_m(y)]\} \times \Gamma(1 - \frac{i}{2}\omega)_1F_1(\frac{i}{2}\omega, 1; \frac{i}{2}\omega y^2) \tag{30}$$

$$x_m = \frac{y + (y^2 + 4)^{1/2}}{2} \tag{31}$$

$$\phi_m(y) = \frac{(x_m - y)^2}{2} - \ln x_m \tag{32}$$

Here both x and y are position parameters describing the source position with Einstein radius as the unit because the normalization constant is chosen as $\xi_0 = \sqrt{\frac{4M_L D_L D_{LS}}{D_S}}$:

$$x = \frac{\xi}{\xi_0}, y = \frac{\eta}{\xi_0}\frac{D_L}{D_S} \tag{33}$$

η is the position parameter, M_L is the red-shifted lens mass and ω is a frequency parameter to distinguish the apparent diffraction region from the strong lensing region:

$$M_{Lz} = M_L(1 + z_L), \omega = 8\pi M_{Lz} f \tag{34}$$

Combining Eq.28 and 34 gives the apparent diffraction region of $\omega < 1$ and obvious magnification region $\omega > 1$. In the region of $f \geq \frac{1}{M_{Lz}}, \omega \geq 1$, the magnification factor in 30 will be converged to the geometric limit:

$$F(f) = \mid \mu_+ \mid^{1/2} - i \mid \mu_- \mid^{1/2} e^{2\pi i f \triangle t_d} \tag{35}$$

$$\mu_\pm = \frac{1}{2} \pm \frac{y^2 + 2}{2y(y^2 + 4)^{1/2}} \tag{36}$$

$$\triangle t_d = 4M_{Lz}[\frac{y(y^2 + 4)^{1/2}}{2} + ln(\frac{(y^2 + 4)^{1/2} + y}{(y^2 + 4)^{1/2} - y})] \tag{37}$$

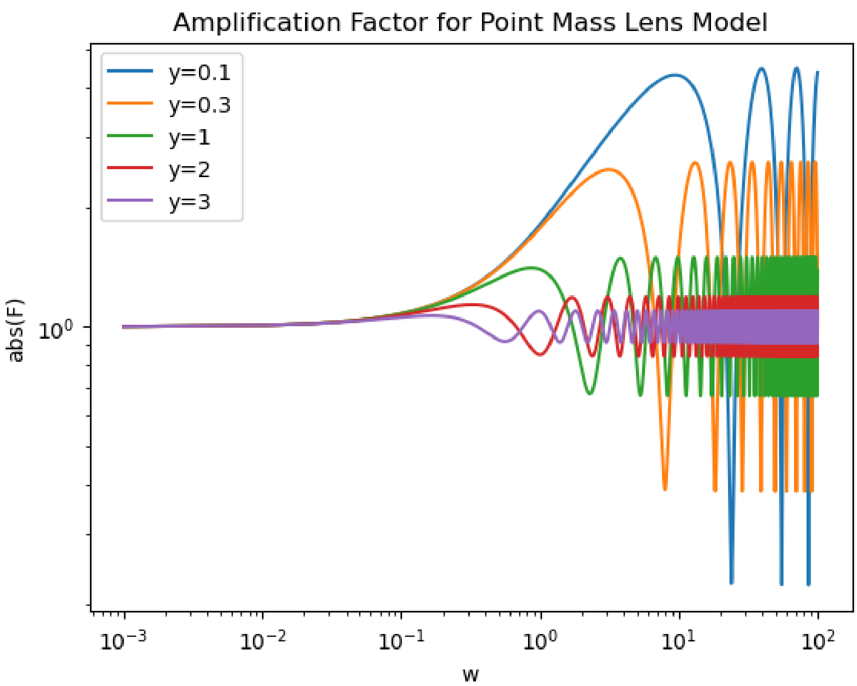

Figure 6: Reconstruction of how the amplification factor changes with frequency parameter ω when position parameter y is fixed.

Fig.6 shows how the amplification factor changes with frequency parameter $omega$ when position parameter y is fixed. When $\omega \leq 1$, the diffraction effect is important and large wavelength λ leads to a small amplification. When $\omega \geq 1$, the interference effect leads to the oscillation behavior. Besides, the region of $\omega >> 1$ sees great oscillation behavior, which means the magnification will be very sensitive to the change in GW frequency.

When it comes to the position parameter y, y=(0,1) refers to the region inside the Einstein radius, and y=0 is when the source is just behind the lens, i.e. the high alignment case. Fig.6 shows a larger magnification factor at a smaller y.

4.2.2 *Different Lensing Type For Moving Cases*

According to *D'Orazio and Loeb 2020*, during the observable lifetime of the moving source (inner BBH), lensing cases can be classified into three different types by comparing several time scales. These time scales include outer orbit period P_o, which is the inverse of outer orbital frequency $P_o = 1/f_0$); time in the band τ_{obs}, which refers to the time when GW emitted from inner BBH is above a set SNR (signal-to-noise ratio); and window crossing time τ_{lens}, which is the time the source needs to cross the Einstein radius of the lens. If the outer orbit is bound, P_o can be calculated by Kepler's Law in the Newtonian case. The window crossing time can be derived by $\tau_{lens} = \frac{\xi_E}{v_{orb,o}}$, ξ_E is the Einstein radius for the lens, and $v_{orb,o}$ is the outer orbital velocity when the source is inside the window. τ_{obs} is related to the LIGO or LISA sensitive band. Then three different lensing cases can be defined as:

- Repeated-lensing: $P_o \leq \tau_{obs}$
- Slowly Moving Lensing: $\tau_{lens} \leq \tau_{obs} \leq P_o$
- Stationary Lensing: $\tau_{obs} \leq \tau_{lens}, \tau_{obs} \leq P_o$

Part III

LENSING IN MOVING TRIPLE BH SYSTEM

5

OBVIOUS LENSING WINDOW

Amplification factor F is a crucial factor to be calculated in order to get the lensed GW signal. In the previous section, Eq.30 shows amplification factor is a function of both frequency parameter ω and position parameter y. Fig.6 shows how the amplification factor changes with fixed y but various ω, each line in it can be considered as BBH evolving at the same position, i.e. COM doesn't move.

So the natural question is what will happen if we fix the ω but change the position y?

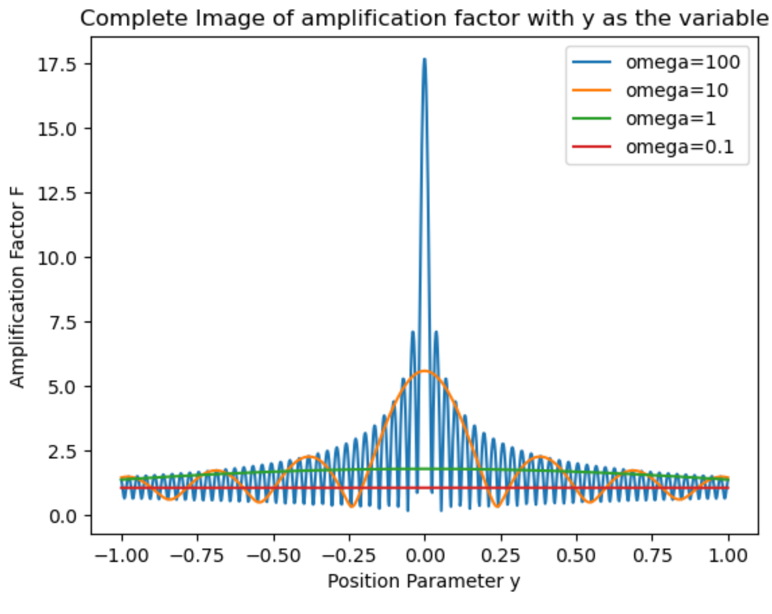

Figure 7: Figure of how the amplification factor changes with position parameter y when frequency parameter ω is fixed.

Fig.7 shows how the amplification factor changes with position parameter y when frequency parameter ω is fixed. Each line gives the changing trend of amplification factor F at a certain ω value of 0.1, 1, 10 and 100. It can be seen when the ω is smaller than 1, the amplification factor F almost doesn't change with y, and both for $\omega = 0.1$ and $\omega = 1$ case the F are very close to 1, leading to the magnification not obvious, which is consistent with the previous results.

When ω is larger than 1, apparent oscillation behavior of the magnification value occurs. The obvious amplification effect, which means $F > 1$ happens in the region of $|y| < 1$. Since $y = \frac{\eta}{\xi_0}\frac{D_L}{D_S}$, $D_L \sim D_S \sim 1Gpc$, $D_{LS} \leq 1$AU and $\xi_0 = \theta_E D_L$, $|y| < 1$ refers to the region inside the Einstein radius. When $|y| > 1$, there is still oscillation behavior but the F value is smaller than 1 so the magnification gradually vanishes. Therefore, Einstein angle θ_E (Eq.26) and corresponding Einstein radius $\xi_E = \theta_E D_L \sim \theta_E D_s$ can be used to define the obvious lensing window: $\theta < \theta_E$, $|y| < 1$ or $|\eta| < \xi_E$, here θ is the angular position of the source (COM of the BBH). As a result, the window boundary is defined as $\theta = \theta_E$, $|y| = 1$ or $|\eta| = \xi_E$.

6

BBH EVOLUTION PROPERTIES

Peter's BBH evolution equations 13,14 lead to how the SMA changes with eccentricity e in Fig.2. In our project, we use Python *odeint* to solve these differential equations. In order to test the accuracy of the numerical calculation, we compare the a(e) in Fig.2 with our simulation calculation results in Fig.8:

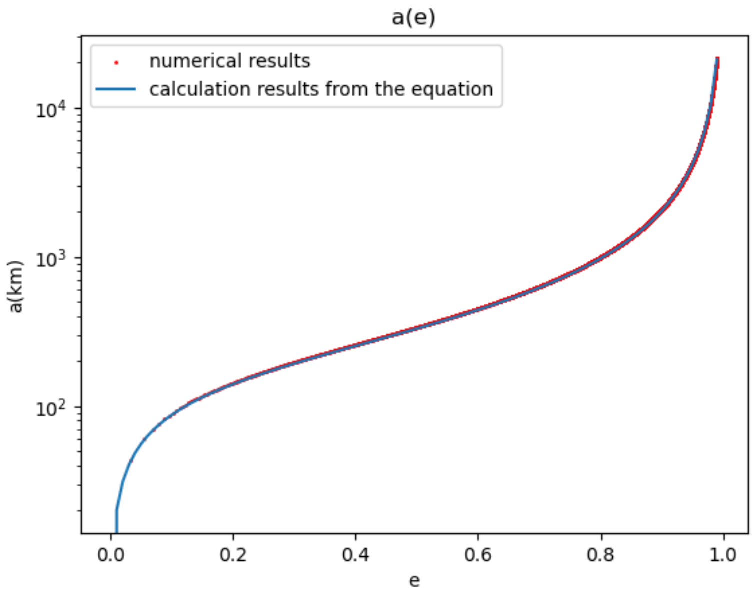

Figure 8: Compare semi-major axis a as a function of the eccentricity e during the binary evolution from numerical and analytical calculation method. The parameters for the BBH is $m_1 = m_2 = 10M_\odot$, initial eccentricity $e_0 = 0.99$ and initial period as $P_0 = 12s$.

The red points come from the numerical calculation and the blue continuous line is from plotting Eq.18. c_0 depends on the initial conditions of the BBH. By testing several values, we finally use $c_0 \sim 370$. The numerical calculation satisfies the analytical results well for the most part. However, we lack abundant values when e is close to 0.

If we choose initial eccentricity as $e_0 = 0.999$, the SMA and eccentricity evolution are shown in Fig9. The lifetime of the BBH with this parameter has a very short lifetime, and during the final stage, both the eccentricity and the SMA decay very rapidly. Compared with Fig.8, the a(e) figure shows some unsmooth when $e \sim 0$, which is a consequence of both Python numerical methods to solve differential equations and sample numbers we choose. It is not a very stable method to solve these differential equations by *odeint*, especially when $e_0 \geq 0.999$.

Next, we will compare the evolution time and process with different initial conditions in Fig.10 11 12 13. Figure 10 and 11 show the evolution of the period and eccentricity respectively with the same initial period P_0 but different eccentricity e_0. Larger e_0 will lead to a more rapid merger. The line parallel to the horizontal axis refers to the BBH already merged so both the period and eccentricity are equal to 0. By comparing the line of $e_0 = 0.1$ and $e_0 = 0.5$, it is apparent that smaller e_0 means the BBH will maintain this eccentricity for a longer time and only at the end of its lifetime both the period and eccentricity decrease rapidly, which is consistent with the inspiral phase and final merger phase for the binary black hole. Figure 12 and 13 show the evolution of the period and eccentricity respectively with the same eccentricity e_0 but different initial period P_0. The larger P_0 is, the longer lifetime the BBH will have.

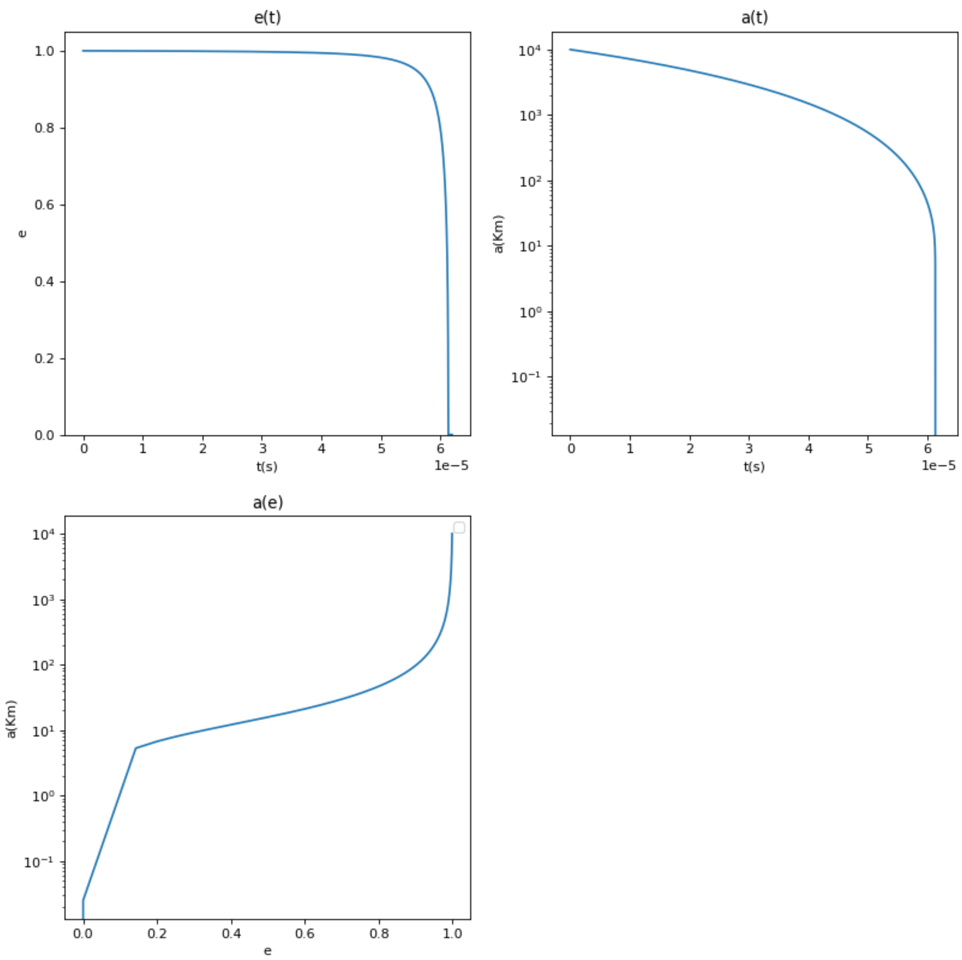

Figure 9: The evolution of a binary black hole by solving the differential equations derived from Peter's equation. The figure shows the evolution of a BBH with $m_1 = m_2 = 10M_{\odot}$, initial eccentricity $e_0 = 0.999$ and initial SMA (semi-major axis) as $a_0 = 10^7 m$.

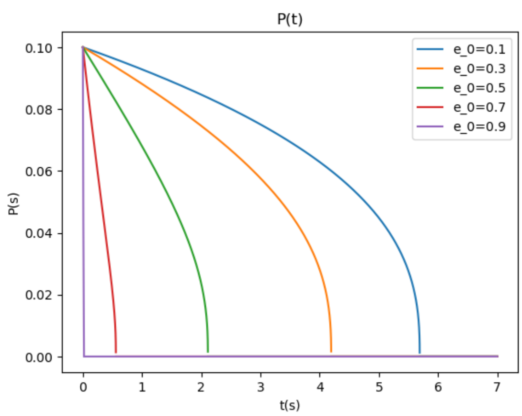

Figure 10: Period evolution with same initial period P_0 but different initial eccentricity e_0.

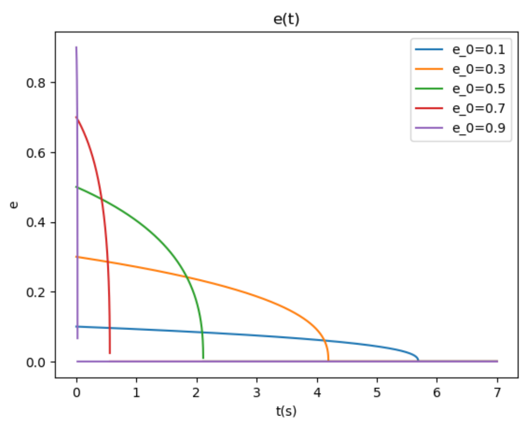

Figure 11: Eccentricity evolution with same initial period P_0 but different initial eccentricity e_0.

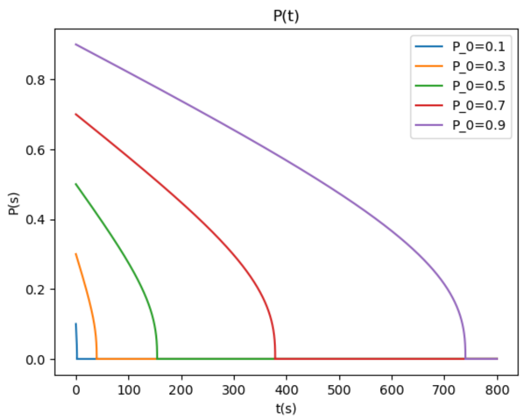

Figure 12: Period evolution with different initial period P_0 but same initial eccentricity e_0.

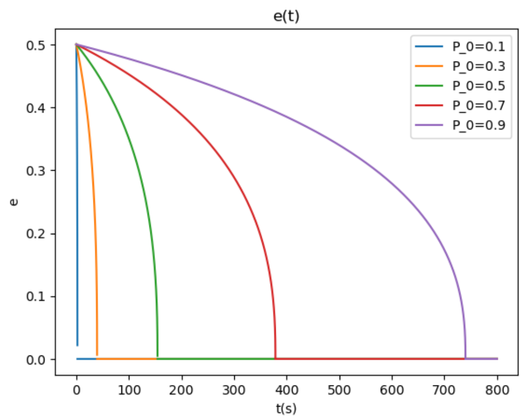

Figure 13: Eccentricity evolution with different initial period P_0 but same initial eccentricity e_0.

7

MOVING CASES

7.1 SIMULATION METHOD

The amplification factor is the main lensing difference between the static and moving cases. In the static case, the source position is considered as the fixed position so the amplification factor is described as $F(t) = F[\omega(t), y]$, $\omega(t)$ depends on the source BBH evolution. However, in the moving case, due to the relative motion between the source and the lens object, the magnification is described as $F(t) = F[\omega(t), y(t)]$. So for a moving case, we need to combine both the motion effects as well as BBH evolution. To be more specific, $\omega(t) = 8\pi M_L f_{GW}$ can be derived from Peter's equations 13,14, y(t) is highly related with the actual orbits.

Regarding the possible lensing results for moving cases with circular orbit, we still need to concentrate on the ratio between window passing time and total orbital time. According to Eintein angle calculation equation Eq.48, if we choose $M_L = 10^5 M_\odot, D_L \sim D_S \sim 1Gpc, D_{LS} = 0.1AU$, $1Gpc = 4.8 \times 10^{14} AU$ and $1arcsec = 1.5 \times 10^{-6}\pi$, then $\theta_E = 2.98 \times 10^{-17}\pi$, the corresponding angular position between source and lens is $\beta = \frac{D_S}{D_{LS}}\theta_E = 0.14\pi$, which is a small angle. As a consequence, the possible lensing types when combining BBH evolution include:

- The merger point is located at the window boundary $y = \pm 1$.
- The merger happens inside the window $|y| < 1$.

- The merger happens outside the window $|y| > 1$. To be more specific, cases include: 1. The binary passes the window and merges outside the window. 2. The binary merged before it entered the window.

Because different parameter combinations (M_1, M_2, M_3, D_{LS}, and starting point) will lead to different lifetime and merger points, it is difficult to set the actual starting point as our starting point (t=0) because we cannot make sure whether the binary enters the window or where is the merger point. One solution is to make the binary evolve backward. To be more specific, we fix the merger (ending) point and make time-reverse simulations, which means the starting point is t=0 (the actual merger point) and the ending point is $t = -T$, T is the total time which BBH needs to evolve from $a = a_0$ to $a \sim 0$, a is the semi-major axis of the inner BBH.

Therefore, the simulation can be divided into the following four steps:

1. Set the initial conditions, including the angular diameter distance D_L, D_S, D_{LS}, the initial and eventual frequency f_0 and f_{end}, the ending point position as well as the mass combination M_1, M_2, M_3 ($M_3 = M_L$).

2. Set time steps to make BBH evolve and SMA evolve from a_0 to a_{end}, then a(t), f(t), and corresponding $\omega(t)$ will be calculated.

3. Select different orbits in which inner BBH moves along. $\eta(t)$ and equivalent y(t) will be got in this step.

4. Combine $\omega(t)$ and y(t) to calculate F(t).

For the second step, we need first to calculate a_0 and a_{end} from f_0 and f_{end}. From Eq.53, if the inner BBH has a circular orbit the dominant frequency emitted should be $f = \frac{\sqrt{GM}}{\pi}\sqrt{\frac{1}{a(t)^3}}$, so:

$$a(t) = (\frac{1}{f^2(t)}\frac{GM}{\pi^2})^{1/3} \tag{38}$$

Therefore the value region for a is $[a_0, a_{end}]$, $a_0 = a[f(0)], a_{end} = a[f(end)]$. Next, we need to set the time steps to make BBH evolve from $a = a_0$ to $a = a_{end}$. According to Fig.9, when the evolution is closer to the merger, the changes on both SMA and dominant frequency will be more rapid. So we should choose time steps in the log scale to make enough points describing the final stage changes such as in Fig.14:

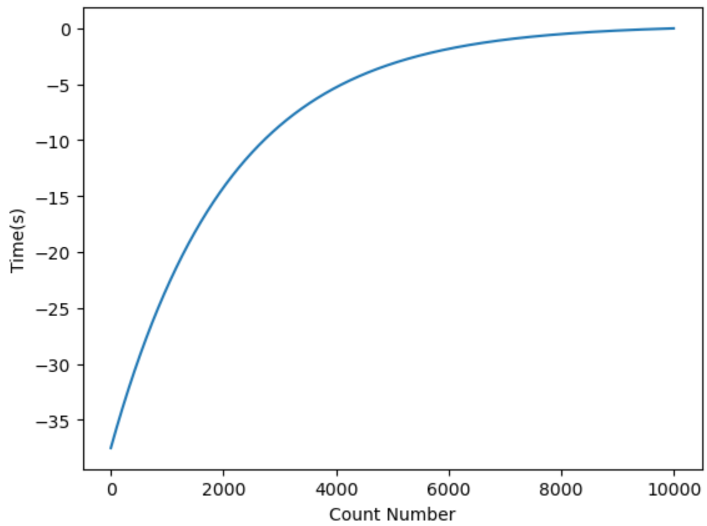

Figure 14: One of the time step selections in our simulation for $M_1 = M_2 = 10M_\odot, M_3 = 10^5M_\odot, D_L \sim D_S \sim 1Gpc, D_{LS} = 0.01AU, f_0 = 10Hz, f_{end} = 60Hz$. In this figure t=0 refers to the ending point and $t \sim -35$s refers to the actual starting point.

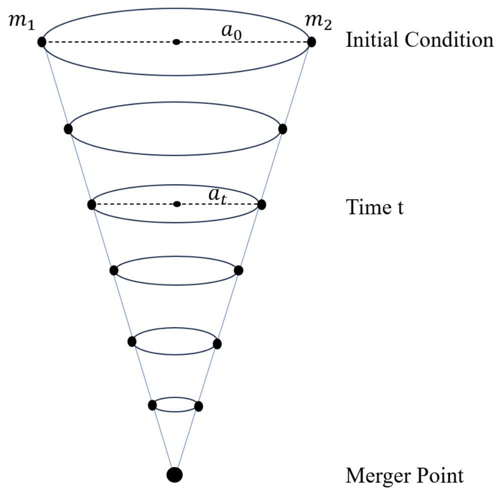

Figure 15: Schematic figure to show the time list and corresponding SMA list a(t).

Since the sampling points are scattered rather than continuous, we are considering several BBHs with virtual full orbit at each time point, leading to a corresponding SMA list a(t) such as Fig.15

shows. Once we have the SMA list a(t), we can also get the frequency list $f(t) = \frac{\sqrt{GM}}{\pi}\sqrt{\frac{1}{a(t)^3}}$ and corresponding ω list $omega(t) = 8\pi M_L f(t)$ for natural unit system and $omega(t) = 8\pi M_L f(t)\frac{G}{c^3}$ for ISU.

For the third step in our simulation, we need to consider the motion and different orbits, along which the inner BBH moves. The simplest case includes CC (both inner and outer orbits are circular) and straight case (inner BBH moving trajectory is straight) shown in Fig.16. For simplicity, we only consider the Newtonian motion here.

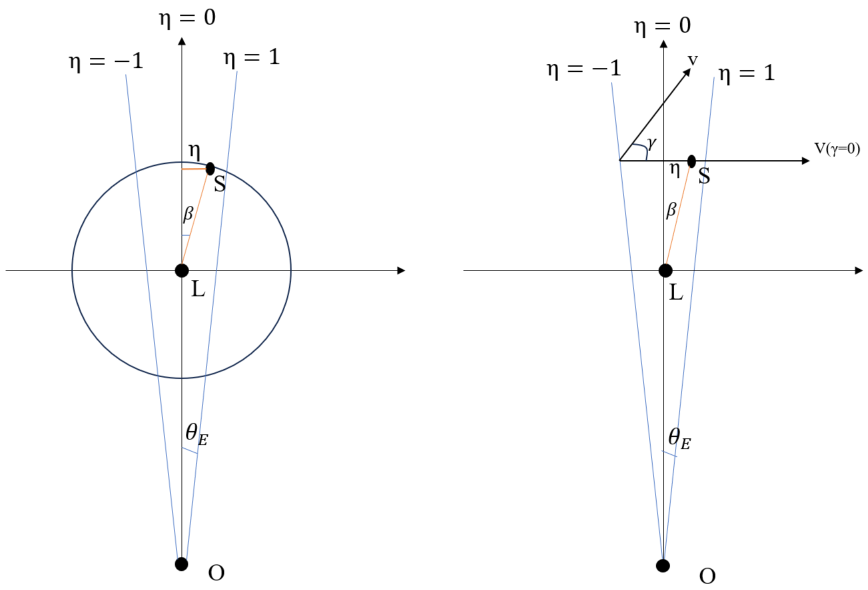

Figure 16: Schematic figure to show different cases, including C-C (both inner and outer orbits are circular) and straight orbit with certain velocity angle.

7.2 CC CASE

For the CC case, we use the angle β to represent the relative angular position between the COM of inner BBH and the lens BH. Since for outer circular orbit $D_{LS} = r_c$, here r_c is the radius of the outer orbit, the Einstein angle $\theta_E = \sqrt{\frac{D_{LS}}{D_L D_S}\frac{4GM}{c^2}}$ will be a constant during the motion. Therefore the position parameter $y(t) = \frac{\eta(t)}{\xi_0}\frac{D_L}{D_S}$ only relates with $\eta(t)$. If we set the ending point as $\beta = \beta_0$, then the $\eta(t)$ is calculated as:

$$\Omega = \frac{2\pi}{T_{out}} \tag{39}$$

$$T_{out} = 2\pi\sqrt{\frac{D_{LS}^3}{G(M_1 + M_2 + M_3)}} \tag{40}$$

$$\beta(t) = \beta_0 + \Omega t \tag{41}$$

$$\eta(t) = \frac{\beta(t) D_{LS}}{\theta_E D_L} \tag{42}$$

Mention that if the left boundary $\eta = -1$ is the ending point, $\beta_0 = -\beta_{max}$ and $\beta_{max} = \frac{D_L}{D_{LS}}\theta_E$. We choose parameter combination $M_1 = M_2 = 10M_\odot, M_3 = 10^4 M_\odot, D_L \sim D_S \sim 1Gpc, D_{LS} = 0.1AU$ as an instance here. In order to avoid *math range error* due to large ω value in Python, we choose initial frequency and ending frequency as $f_0 = 10Hz, f_{end} = 500Hz$, which means the ending point is near the actual merger point but not the exact one. Then if the ending point locates at the window boundary $\eta = -1$ and the incoming direction is from $\eta = 1$ to $\eta = -1$, the amplification factor F(t) and position $\eta(t)$ will be shown in Fig.19:

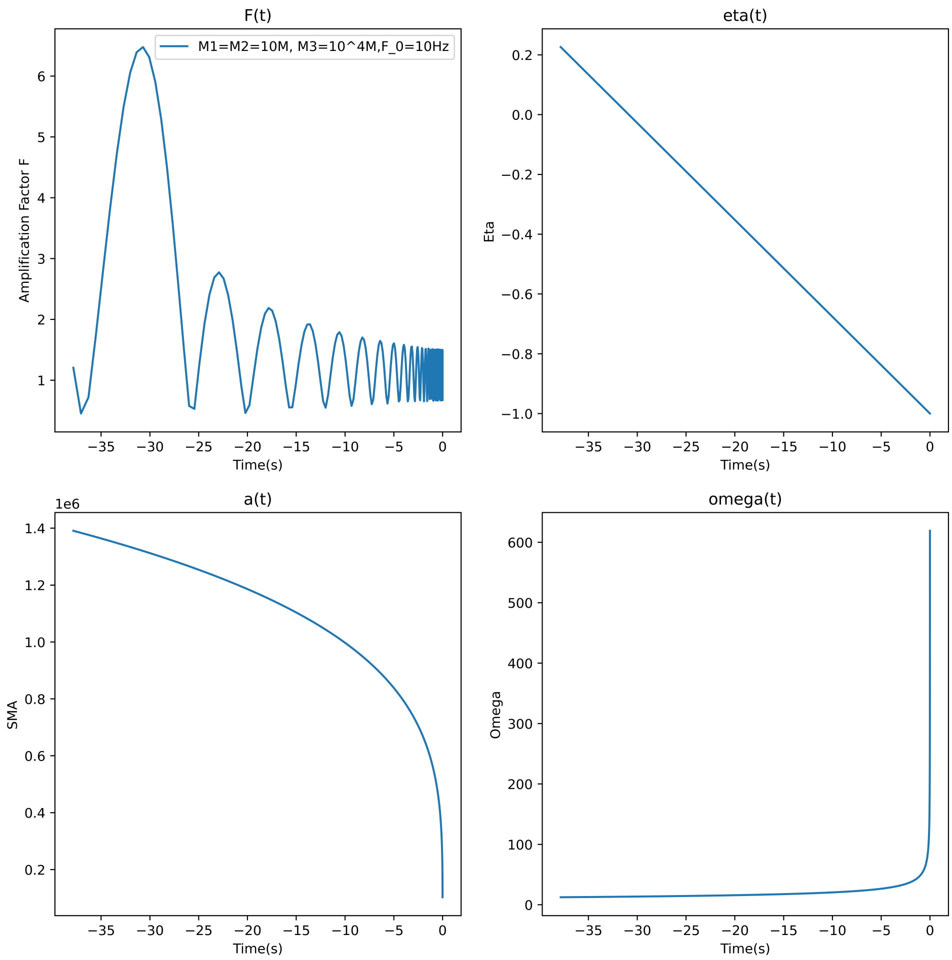

Figure 17: If the ending point is $\eta = -1$, the lifetime from $f_0 = 10Hz$ to merger is approximately 37s for a BBH with $M_1 = M_2 = 10M_{\odot}$. The SMA evolution is consistent with the results of Peter's equations. For the circular orbit, the starting point will be close to $\eta = 0.2$.

The next step is to change the ending point from $\eta_{end} = -1$ to $\eta_{end} = 0.4$ which is shown in Fig.18, representing the case when a merger happens inside the window. Comparing Fig.19 and 18 sees under this parameter combination choice, the $\eta(t)$ changes linearly, so the circular orbit section inside the window is equivalent to the straight motion. When the COM of inner BBH passes $\eta = 0$ during its evolution period, the amplification factor value peak occurs at the $\eta = 0$ point.

However, if the inner BBH doesn't pass $\eta = 0$ during its evolution period, which means $\eta_0 > 0$ and the moving direction is from $\eta > 0$ to $\eta < 0$, then the amplification factor value peak occurs at the final stage of its evolution. Except for the case when the ending point is exactly at $\eta = 0$, there will also be some oscillation behavior at the final evolution stage.

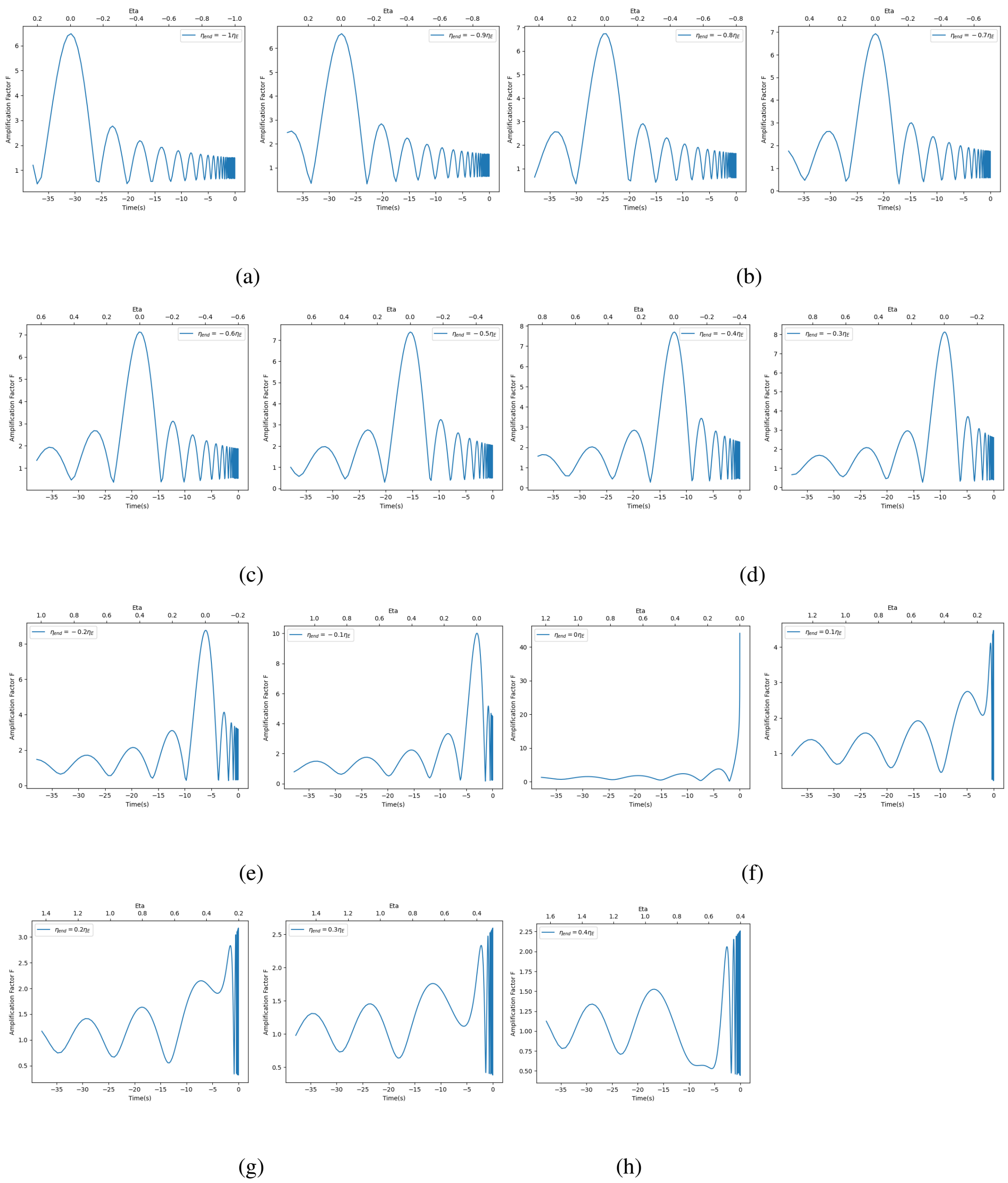

Figure 18: Different amplification factor results for CC case when the ending point changes from $\eta_{end} = -1$ to $\eta_{end} = 0.4$, which represents several cases when the merger happens inside the obvious magnification window. The bottom axis is the evolution time, t=0 refers to the ending point, and $t \sim -37s$ is the starting point.

7.3 STRAIGHT CASE

For the straight case, we set the ending point is inside the region $\eta \in [-1, 0)$. For simplicity, the constant velocity is equal to the orbital velocity for the CC case with the same parameter combination

$v_{str} = v_{CC}$. The main differences between CC and straight case include: 1. The $\eta(t)$ are different at each same time due to the orbital curvature, but how large is the difference depends on the actual parameter combination and velocity angle γ. 2. The angular diameter distance between source and lens D_{LS} are changing for the straight case, but in the CC case, it is a constant parameter. As a consequence, we need to make some changes when it comes to the simulation codes for straight cases.

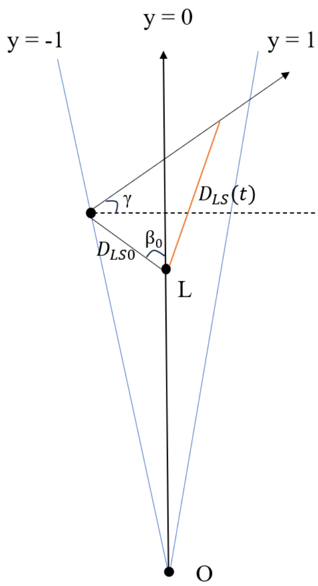

Figure 19: Schematic figure of how to calculate the $D_{LS}(t)$ in the straight case.

If the angle between the velocity direction and the horizontal axis is γ, the ending point is located at the window boundary y=-1, the incoming direction is from y=1 to y=-1, then the $D_{LS}(t)$ is calculated as Eq.43 according to the cosine theorem:

$$D_{LS}(t) = \sqrt{(vt)^2 + (D_{LS0})^2 - 2(vt \cdot D_{LS0}) \cdot cos(\gamma + \frac{\pi}{2} - |\beta_0|)} \tag{43}$$

Then the Einstein radius and corresponding position parameter η at time t are:

$$\theta_E(t) = \theta_E = \sqrt{\frac{D_{LS}(t)}{D_L D_S} \frac{4GM}{c^2}} \tag{44}$$

$$\eta(t) = \frac{D_{LS0} \cdot sin(\beta_0) + v_{str} \cdot t}{D_L \cdot \theta_E(t)} \tag{45}$$

8

DISTINGUISH DIFFERENT MOVING ORBITS

The previous section has shown that in order to get F(t) for moving cases, we need to first concentrate on $\omega(t)$ and y(t). $\omega(t)$ can be directly obtained from Peter's equation, however, y(t) is highly dependent on the orbital types, since different trajectories will have different orbital curvature and passing time inside the obvious magnification window. Even for the same kind of orbit, for instance, the eccentric orbit, different inclination angles will lead to differences inside the window, just as Fig.20 shows.

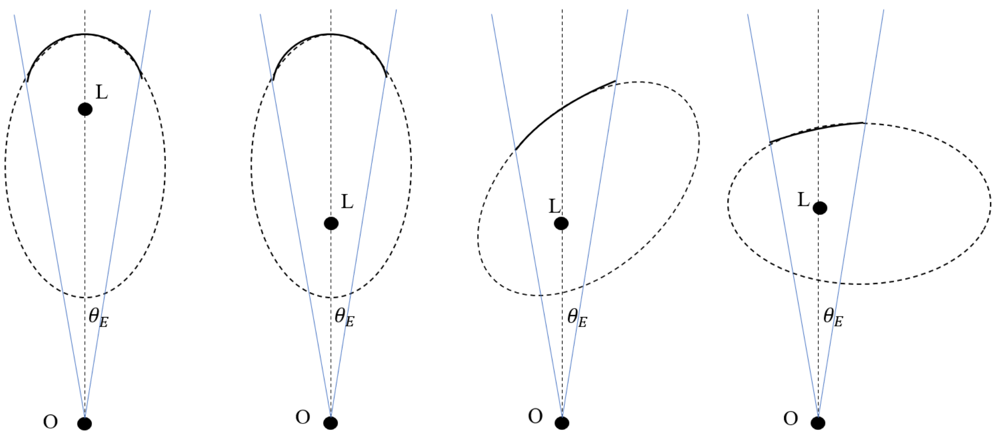

Figure 20: Schematic figure shows the same eccentric orbit with different inclination angles will lead to difference inside the window. These differences include both orbital curvature and window passing time. Solid lines refer to the orbiting part inside the obvious lensing window.

Then comes the question: how do we distinguish different orbits?

8.1 TWO CHALLENGES

Our next goal is to distinguish different moving orbits for COM of the inner BBH, the specific method is to find whether there is a differentiable difference between the magnification factor of difference. So we choose the same initial M_1, M_2, M_3, D_L, D_S, D_{LS} and frequency region f_0, F_{end}, but the orbital types are different.

8.1.1 *High ω*

The first challenge comes from the high ω. BBH dominant frequency Eq.53 shows during the lifetime of a BBH, the dominant frequency will increase continuously until the merger happens. Since $\omega = 8\pi M_L f G/c^3$, the *omega* will also increase continuously.

According to the simulation results, if we choose the initial frequency as $f_0 = 10Hz$ for a system of $M_1 = M_2 = 10M_\odot, M_3 = 10^5M_\odot, D_L \sim D_S \sim 1Gpc, D_{LS} = 0.1AU$, the initial ω is around 123 and will be increased by several orders of magnitude in the subsequent evolution. If the lens mass is larger than this lens value, $M_L = 10^5M_\odot$, the ω increases even faster according to Eq.48. In order to avoid the *math range error* in Python when calculating the amplification factor, we need to also set a maximum value for the frequency and corresponding ω value. Therefore, the ending point in our simulation is not the actual merger point, but some point in the final stage and close to the actual merger point.

8.1.2 *High Oscillation Behavior*

Another challenge comes from the high oscillation behavior when $\omega > 1$. High oscillation behavior means the amplification factor is very sensitive to both position changes and ω changes. In the following part, we will select several examples to see whether we can analyze the difference.

Here is one of the examples with 10000 sample points:

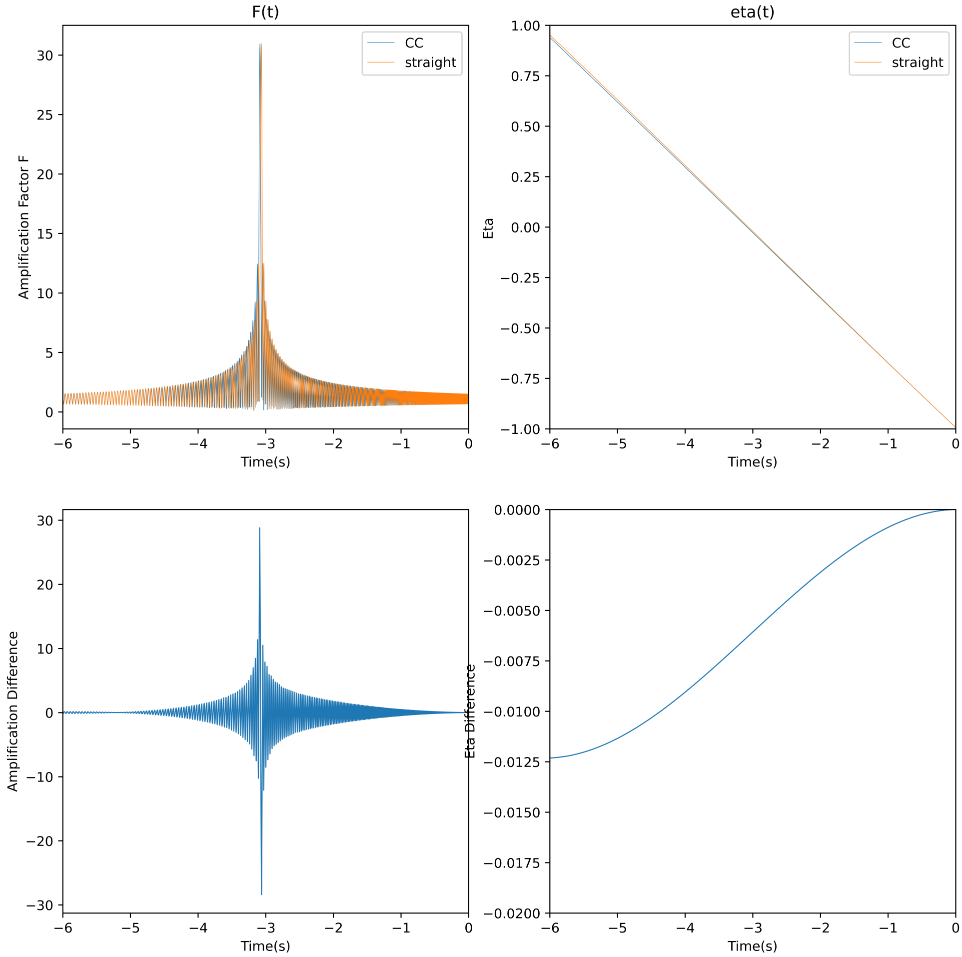

Figure 21: Direct simulation results of amplification factor F(t) and position parameter $\eta(t)$ for CC (inner circular orbit + outer circular orbit) and straight orbit case. The two bottom figures show the difference of F(t) and $\eta(t)$ respectively. The parameter we choose here are: $M_1 = M_2 = 10M_\odot, M_3 = 10^5 M_\odot, D_L \sim D_S \sim 1Gpc, D_{LS} = 0.01AU$.

8.2 TWO COMPARISON METHOD

8.2.1 *Time Average Comparison*

One way to separate the 2 different cases under such a high oscillation behavior is to represent the results by average values. To be more specific, time points should be separated into several groups, and the amplification value in each time group is the average value of all the corresponding F values inside the group. So here comes the question: how to cut the time? In our previous code, the time point is not linear but log relation, just as Fig.14 shows.

So there will be two different methods to split the time into several groups:

1. Time Linear Split: The time interval in each group is equal. For example, each group contains the amplification changes in 1s (the interval can also be 0.1s or 0.01s).

2. Time Nonlinear Split: The time number in each group is equal, which means each group has the same number of time points, as a consequence, the time interval is still in the log scale.

In order to relate actual measurements, here we choose the time linear split, which means the time range covered in each group is the same. The time intervals in each group are 1s, 0.1s, 0.05s, 0.04s, 0.03s and 0.01s. Parameter combination is chosen as The parameter we choose here are: $M_1 = M_2 = 10M_{\odot}, M_3 = 10^5 M_{\odot}, D_L \sim D_S \sim 1Gpc, D_{LS} = 0.01AU$, angle velocity $\gamma = 0$. The comparison between CC and the straight moving case is shown in Fig.22. The difference in the time average results is shown in Fig.23.

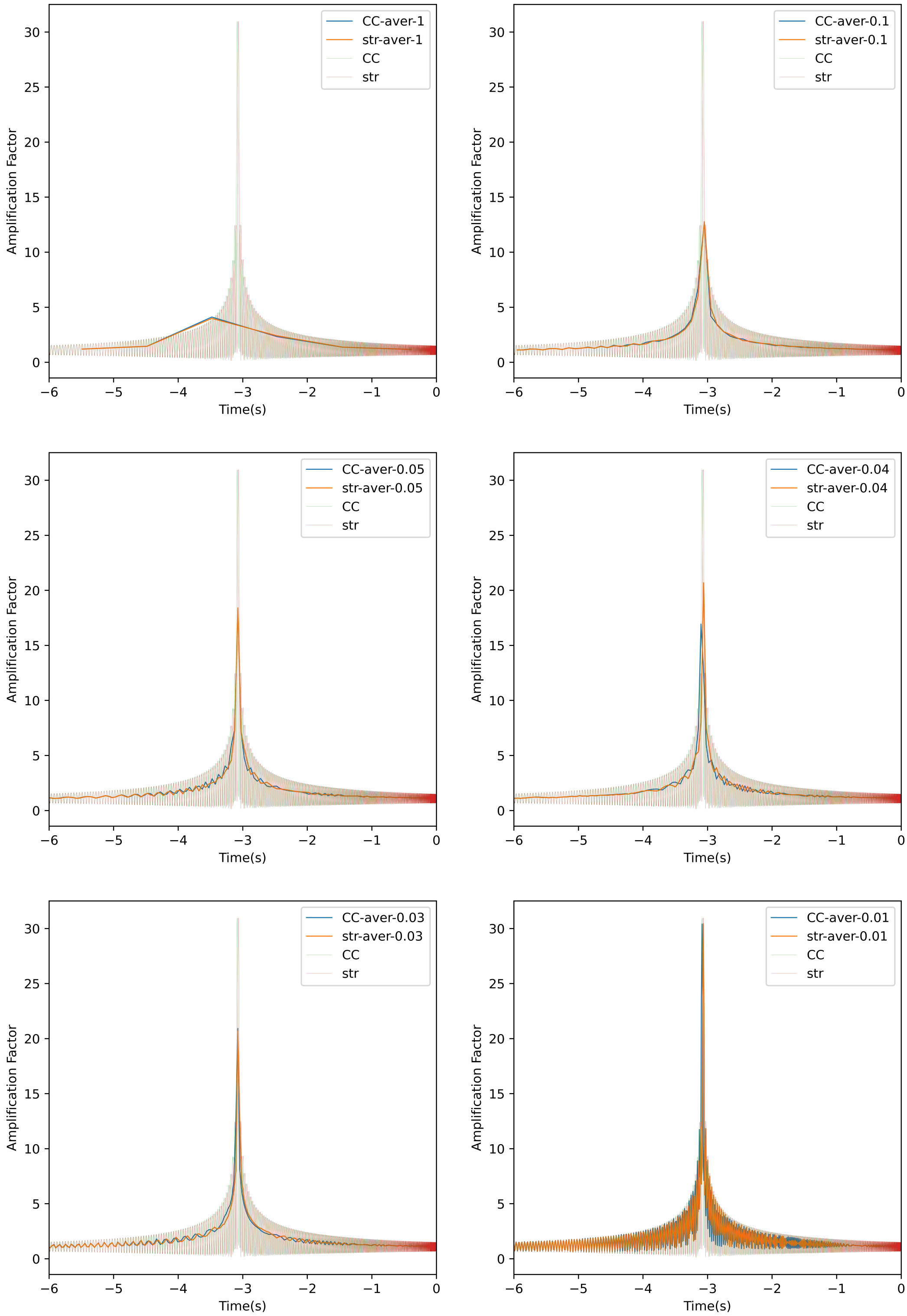

Figure 22: Comparison of two cases under different group numbers. The time intervals in each group are 1s, 0.1s, 0.05s, 0.04s, 0.03s, and 0.01s. Solid lines refer to the time average results, and the background dash lines are the initial amplification factor values for CC and straight case directly from the simulation.

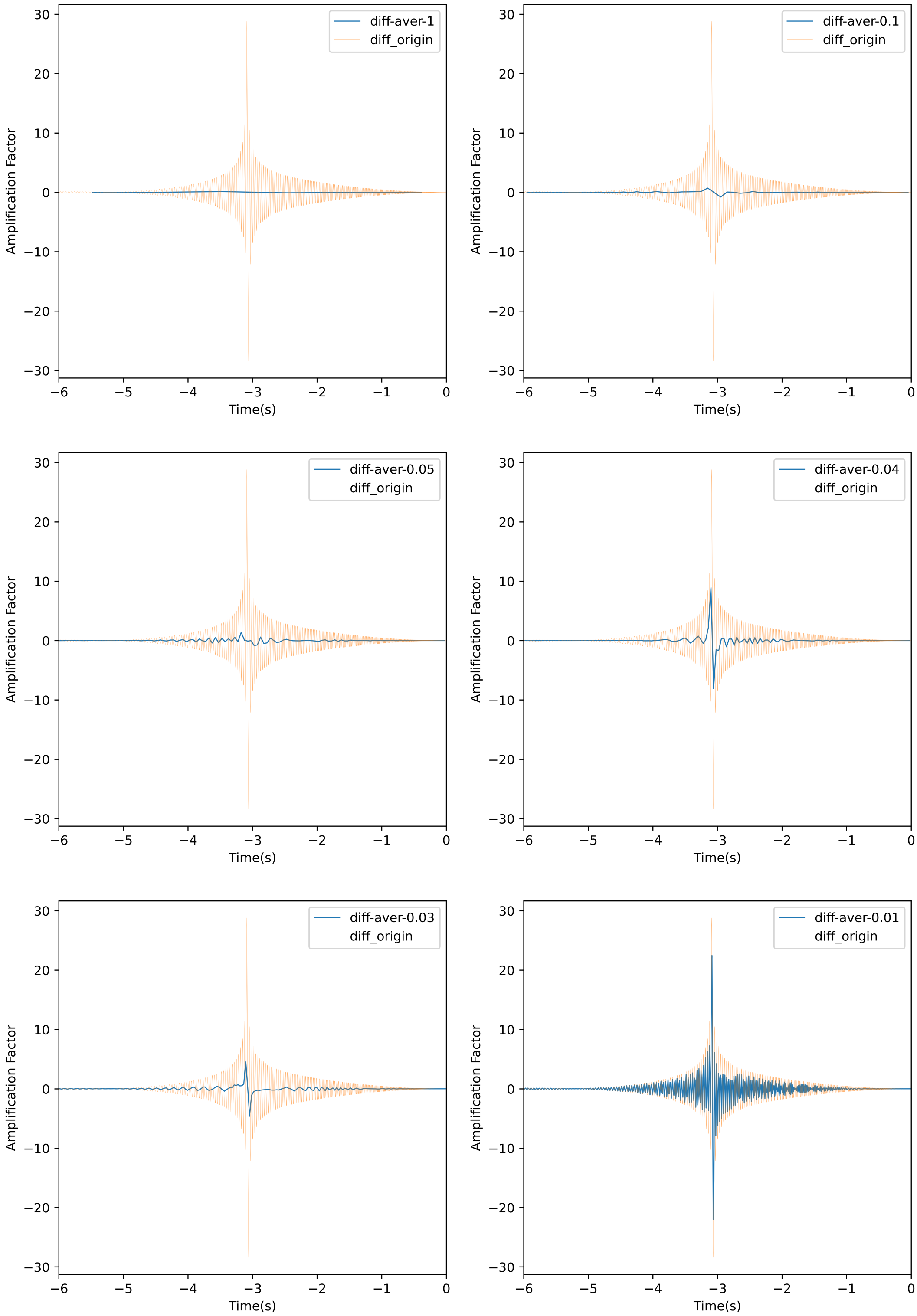

Figure 23: Difference of the time average results for CC and straight case. The time intervals in each group are 1s, 0.1s, 0.05s, 0.04s, 0.03s, and 0.01s. Solid lines refer to the difference of time average results, and the background dash lines are the initial amplification factor value difference.

The two figures above show the amplification factor value is highly related to the sample interval. If the interval is very large, such as $\triangle t = 1s$ in Fig,22, the results even cannot reveal the actual peak magnification position. When the sample interval becomes smaller, such as $\triangle t = 0.01s$, there will be some phase shift between CC and straight case.

Amplification factor value difference also highly depends on the sample interval. In fig.23 it is apparent that the difference is largest when $\triangle t = 0.01s$. However, the difference for $\triangle t = 0.04s$ is larger than $\triangle t = 0.03s$ shows even a little change in the sample interval will lead to results that cannot be ignored.

Previous comparison figures are the results of incoming angle velocity $\gamma = 0$. If we choose different incoming velocities for $\gamma \in [0, 0.5\pi]$, the amplification factor is shown in Fig.24. The line representing $\gamma = 0.5\pi$ doesn't have a magnification peak because this incoming angle means the incoming direction is parallel to the line-of-the-sight, so the position parameter y will never reach the peak position y=0.

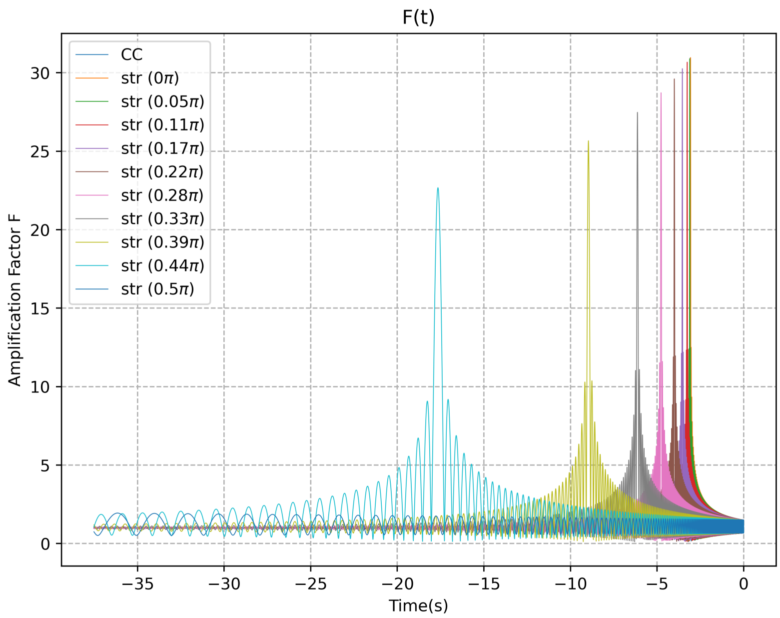

Figure 24: The amplification factor F(t) for CC case and straight case with different incoming velocity γ. The parameter combination is $M_1 = M_2 = 10M_\odot, M_3 = 10^5 M_\odot, D_{LS} = 0.01AU$.

Although Fig.24 shows some difference in the peak magnification position, it will still be difficult for us to separate the outer circular orbit with outer straight orbits at low incoming angles when the inner binary has eccentric orbits. The amplification factors we calculated before are the results when using the dominant frequency of GW emitted from inner BBH. However, the GW frequencies are different for inner circular and eccentric orbit BBH. For the circular case, GWs are equivalent to the twice of orbital frequency, which means all of them are emitted at the lowest-order harmonic n=2 of the orbital frequency. However, for the eccentric orbit case, GWs are a series of harmonics of the orbital frequency. (*Wen 2003*). Since the F value is very sensitive to the frequency in the high oscillation region and the peak position is close to each other at low incoming angles, it will be difficult to separate different orbits.

8.2.2 *Certain ω Region*

Now that high oscillation behavior will lead to a large difficulty in the separation of different orbits, one method is to focus on the region before the amplification factor enters the high oscillation behavior region.

Let us review the figure Fig.6 here. When we focus on one line with changing ω value and fixed y value, we will see a region before it shows oscillation behavior. We can define this region as from when the F value is just larger than 1, to the first few peak region. We define the first peak ω as the ω value when it reaches the first peak. Then the relation between the first peak ω value and position parameter y is shown in Fig.25. The larger y is, the smaller the first peak ω will be, which is consistent with Fig.6 that higher position parameter y will lead the first peak towards the left-hand side.

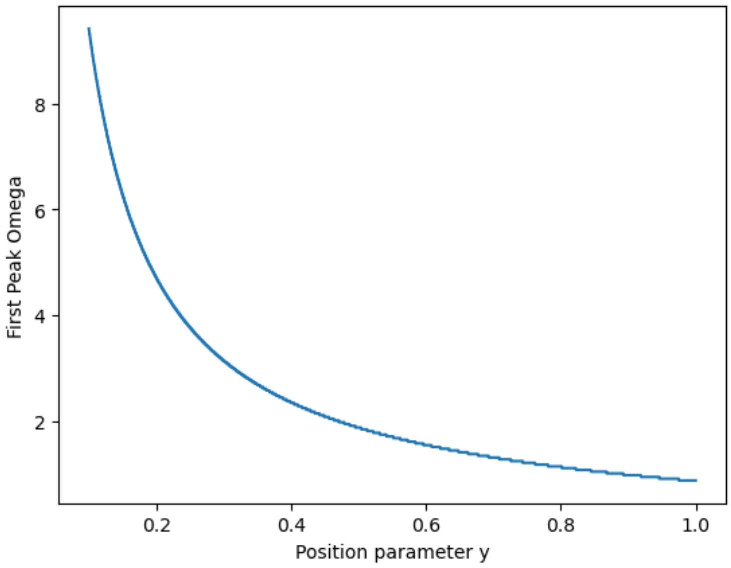

Figure 25: The relation between first peak ω value and position parameter y. The first peak ω is defined as the ω value when it reaches the first peak when the y is fixed.

In the next step, we define the region in which the amplification factor hasn't entered the high oscillation region. It is reasonable to choose region $\omega \in [0.5, 20]$ which contains all the first peak ω values for $y \in [0.1, 1]$. Then comes the question: what is the parameter combination to make both the

ω value inside the region we want and the difference of magnification large enough to separate one orbit from another?

One method is using characteristic time parameters as a criterion for judgment, in order to make the peak magnification inside the window must be included and the window time is roughly comparable to the time inside the ω region we need. So here we choose two time parameters: $P_{win-pass}$, the time when inner BBH is inside the window, and t_ω, the time BBH needs to evolve in certain ω region, for example, $\omega \in [0.5, 20]$.

Now let's calculate the parameters above for the CC case. First for the $P_{win-pass}$:

$$P_{win-pass} = \frac{2\beta_{max}}{\Omega} \tag{46}$$

$$\beta_{max} = \frac{D_S}{D_{LS}}\theta_E \tag{47}$$

Here θ_E is the corresponding Einstein angle and Ω is the angular velocity for the outer orbit:

$$\theta_E = (\frac{M_L}{10^{11.09}M_\odot})^{1/2}(\frac{D_L D_S/D_{LS}}{Gpc})^{-1/2}arcsec \tag{48}$$

$$P_{out} = 2\pi\sqrt{\frac{D_{LS}^3}{G(M_1 + M_2 + M_3}} \tag{49}$$

$$\Omega = \frac{2\pi}{P_{out}} = D_{LS}^{-\frac{3}{2}}\sqrt{G(M_1 + M_2 + M_3)} \tag{50}$$

$$P_{win-pass} = 3 \times 10^{-6}\pi\sqrt{\frac{Gpc}{10^{11.09}M_\odot}}\sqrt{GM_3(M_1 + M_2 + M_3)D_{LS}^2} \tag{51}$$

Next for the t_ω:

$$\omega = 8\pi M_{Lz} f \frac{G}{c^3} \tag{52}$$

$$f = \frac{\sqrt{GM}}{\pi}\frac{(1+e)^{1.1954}}{[a_{in}(1-e^2)]^{3/2}} \tag{53}$$

$$\omega = \frac{8G^{\frac{3}{2}}}{c^3}M_3(M_1 + M_2)^{\frac{1}{2}}a_{in}^{-\frac{3}{2}} \tag{54}$$

$$t_\omega = \frac{a(\omega_{min})^4 - a(\omega_{max})^4}{4\beta} \tag{55}$$

Then we define the criteria for judgment as $\frac{t_\omega}{P_{win-pass}}$, which describes How much part of $\omega \in [0.5, 20]$ is inside the window. One reasonable choice is to set $\frac{t_\omega}{P_{win-pass}} \in [0.5, 5]$, which means the motion

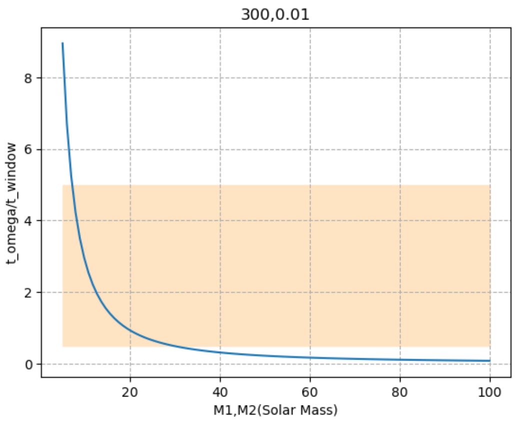

(a) Only change $M_{1,2}$

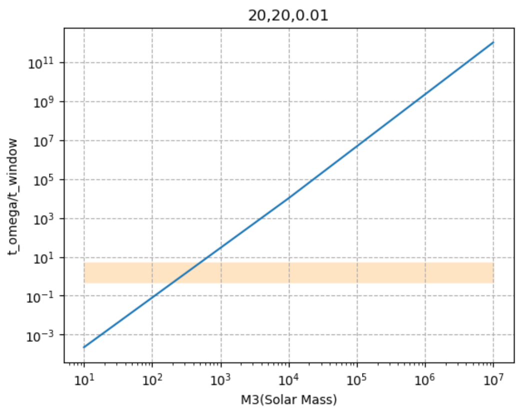

(b) Only change M_3

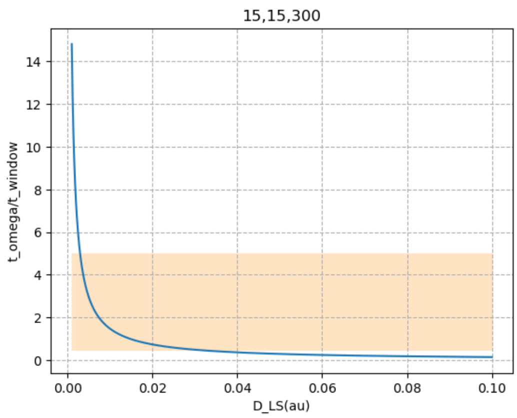

(c) Only change D_{LS}

Figure 26: How the $M_{1,2}, M_3, D_{LS}$ changes the value of $\frac{t_\omega}{P_{win-pass}}$. In each subfigure, we only change one of the three parameters and make the other two fixed.

must cover the largest magnification position $\eta = 0$ and avoid too many sample points outside the window region ($\eta > 1$).

Previous calculations have shown that parameters affecting this time ratio include: M_1, M_2, M_3, D_{LS}. For simplicity, we consider $M_1 = M_2$ so there are three groups of variables. In the following parts, we will show how the three groups influence the value of $\frac{t_\omega}{P_{win-pass}}$ and find the suitable region to satisfy both $\omega \in [0.5, 20]$ and $\frac{t_\omega}{P_{win-pass}} \in [0.5, 5]$.

In each subfigure of fig.26, we only change one of the parameters and make the other two fixed. The fixed values for the other two parameters are shown in the upper titles of each figure. The orange dashes region refers to $\frac{t_\omega}{P_{win-pass}} \in [0.5, 5]$. The overlap region reveals suitable variable values to satisfy our conditions. It is conveyed that M_3 has the largest effect when its value changes a few orders of magnitudes. When M_3 increases, $\frac{t_\omega}{P_{win-pass}}$ increases linearly. However, this time ratio will decrease nonlinearly if either $M_{1,2}$ or D_{LS} increases.

Since all three variables influence the time ratio value monotonically, we are able to combine all three parameters in Fig.27:

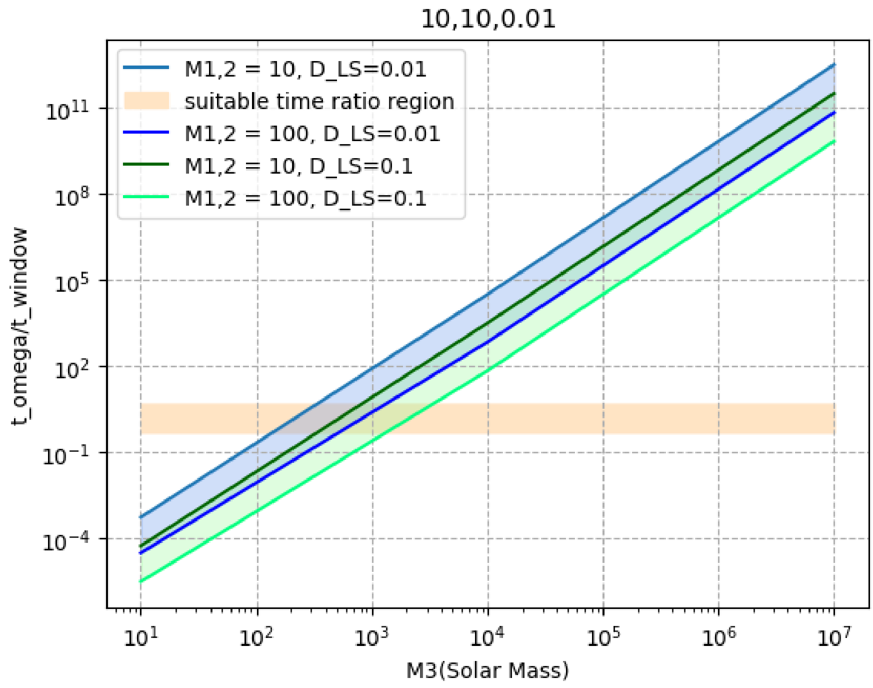

Figure 27: Suitable parameter combination to satisfy both $\omega \in [0.5, 20]$ and $\frac{t_\omega}{P_{win-pass}} \in [0.5, 5]$.

The overlap region gives us the M_3 value if $M_{1,2} \in [10, 100]M_\odot$ and $D_{LS} \in [0.01, 0.1]AU$, in order $\omega \in [0.5, 20]$ and $\frac{t_\omega}{P_{win-pass}} \in [0.5, 5]$. Any parameter combination inside or very close to this band will lead to the binary motion containing the largest magnification inside the window, and ω values inside the window haven't entered the high oscillation region.

Part IV

RESULTS

9

RESULTS

9.1 RESULTS

In this section, we will choose a group of parameters inside the overlap region in Fig.27 and calculate how the position parameter y and amplification factor F change with time t when the incoming direction is different for the straight orbit case, i.e. angle γ is changing. Then we will compare them with the CC case when they have the same orbital velocity.

The parameter we choose is: $M_1 = M_2 = 10M_\odot, M_3 = 700M_\odot, D_L \sim D_S \sim 1Gpc, D_{LS} = 0.1AU$, angle velocity $\gamma \in [0, 0.5\pi]$. Then Fig.28 shows y(t), Fig.29 and 30 shows F(t) for different velocity direction case and F(t) difference when compared with CC case respectively.

y(t) in Fig.28 is consistent with the actual cases when it comes to different incoming angles. If $\gamma = 0$ due to the small Einstein angle and corresponding β angle, the y(t) will be very close to the circular trajectory if the central object mass is not large enough to make a significant orbital curvature difference. If $\gamma = 0.5\pi$, it can be considered as the incoming direction is along the LOS (line-of-the-sight) and y can be considered nearly constant.

Fig.29 and 30 show significant differences among different incoming directions, especially the peak magnification factor position and corresponding peak values. The smaller γ is, the larger the F peak

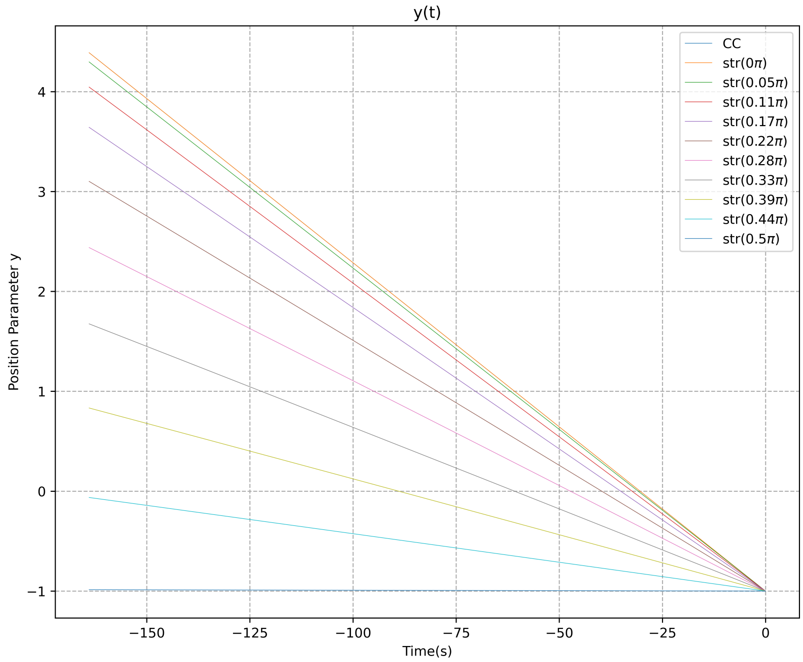

Figure 28: How the position parameter y changes with t for CC and straight orbit case with different incoming directions.

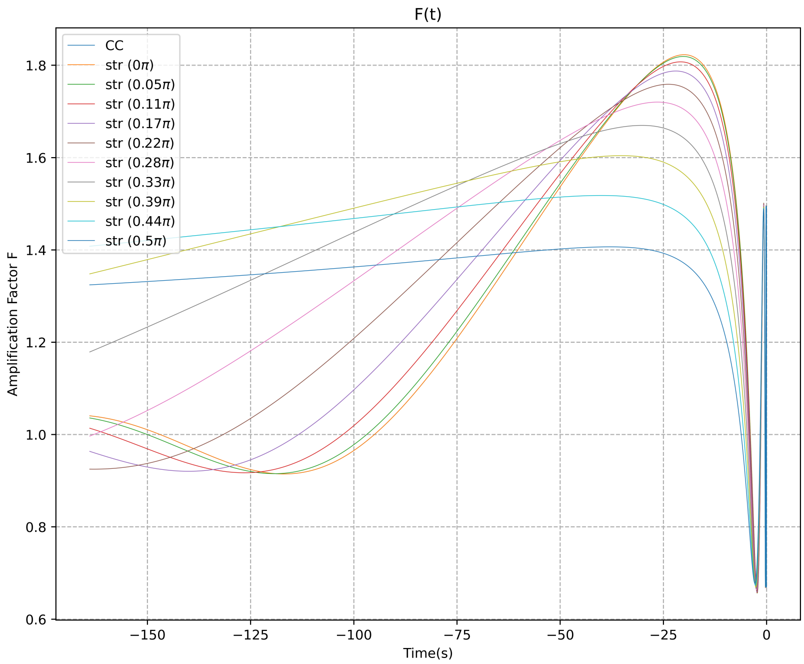

Figure 29: How the amplification factor F changes with t for CC and straight orbit case with different incoming directions.

value will be. Besides, due to the different time inside the window, the rate of change is also different. The orbits close to the CC case show the most active changes.

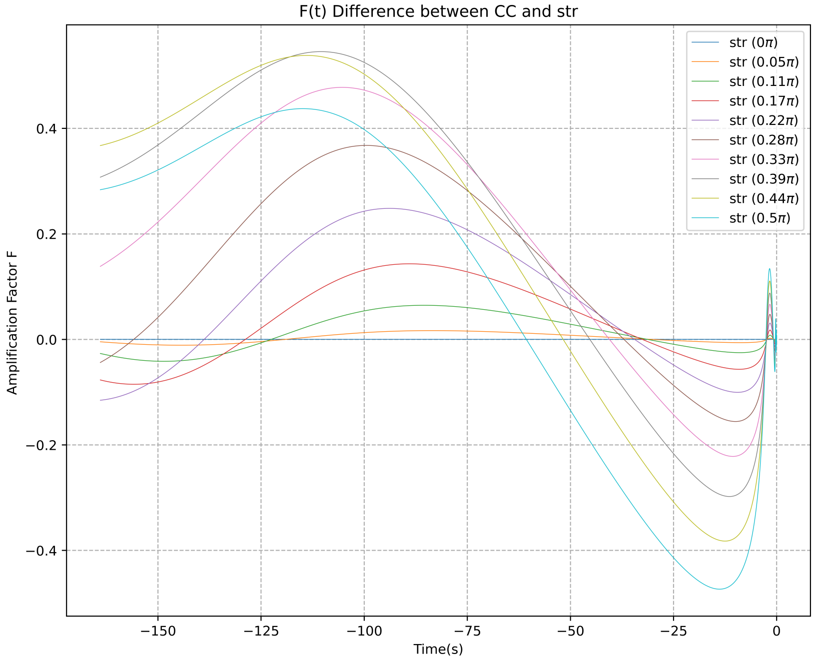

Figure 30: How the amplification factor F changes with t for CC and straight orbit case with different incoming directions.

When it comes to the comparison between different orbits, the most extreme case $\gamma = 0$ still cannot be separated from the circular case due to the lens mass we choose here $M_3 = 700M_\odot$ is not large enough to lead to a significant orbital curvature difference between circular orbit and straight orbit with the same constant velocity. If we combine Fig.27, the lens mass large enough to make significant curvature difference will also lead $\frac{t_\omega}{P_{win-pass}}$ increase several orders of magnitude. If we still want to observe the time for $\omega \in [0.5, 20]$, repeated lensing is also possible to occur.

9.2 DISCUSSION AND FUTURE WORK

A circular orbit is used in this work when we consider the bound orbital motion for inner BBH. However, in actual cases, high eccentricity is the most crucial parameter to distinguish the BBH formation channel between the isolated stellar channel and the gravitational dynamical channel. If we are going to infer the formation channel from the gravitational lensing, inner BBH with high eccentricity is the best choice. This choice will also lead to some challenges, including: a) How to distinguish different orbits. Even for the elliptical orbits with the same SMA and eccentricity, different inclination angles will lead to different orbit parts inside the obvious lensing window. We need to separate different orbits. b) For the eccentric BBH, GW frequency is no longer only twice of the orbital frequency, instead, the actual frequency will be a range of harmonics, which will increase the difficulty of distinguishing different orbits since the high oscillation behavior of amplification factor at high ω region.

Besides, for the motion part when calculating the position parameter y(t), we only consider the case under low-velocity cases with Newtonian methods when it comes to the orbital motion with constant velocity. In future work, we can expand it into the low-velocity case under Post-Newtonian approximation and high-velocity case by using the General Relativity method.

Another possible situation that is not included in this work is Retro-Lensing. One of the possible lensing types mentioned in previous sections is repeated lensing, which refers to several times of lensing if the observation time is larger than both the lifetime of the inner BBH and outer orbital period, and the lifetime of inner BBH is also larger than the outer orbital period. If repeated lensing could happen, it is also possible for retro-lensing to happen. Retro-lensing means when the inner BBH is moving between lens and observer and when they are in highly alignment case, the Gw signal emitted by BBH and towards the lens will be bent with a deflection angle equal to π and finally reaches observer (*Yu et al. 2021*). As a consequence, the final lensed signal received by the observer should be modified by the retro-lensing effect.

Last but not least is other Environmental influences. The tidal effect, and accretion disk around SMBH (supermassive black hole) may also influence the final lensing signal. Besides, in some small probability events, it is also possible for the lensed GW signals to encounter some other massive objects on their path of propagation. These objects can be considered as the second lens, either the point-model lens (compact objects like BH) or the Singular Isothermal Sphere Lens (galaxies, star clusters, etc.)(*Takahashi and T. Nakamura 2003*). Then the final lensed signal observed by the detector is the superposition of two lensing effects. The method to separate signals from only once or twice lensing effect should be down in the future.

10

CONCLUSION

In this project, we mainly focus on the gravitational lensing effect in a hierarchical triple BH system, in which the inner BBH moves along certain orbits around the central BH. The central BH is considered as the gravitational lens and the inner BBH is the source of gravitational waves. GW lensed by the central BH will finally arrive observers and can provide information about the source parameter as well as the orbital type.

Due to the wavelength of GW being much larger than light, the wave effect should be included when calculating the lensed signal. Diffraction will influence the magnification and interference will result in obvious oscillation behavior for the amplification factor. The most crucial factor during the calculation process is the amplification factor since the lensed signal is the product of unlensed signal and amplification factor. This factor is a function of both GW frequency and the source position. According to whether the F is larger than 1 we are able to define the obvious lensing window.

What makes this work different from most other previous work is we consider the lensing effect in moving cases, which means not only the evolution of inner BBH, but also the outer motion ought to be considered in order to calculate the amplification factor. Time is the parameter we use to combine evolution and motion. For the simulation method, we first set the parameter combination including mass, relative angular diameter distance, and frequency at the beginning and the end. Then we simulate the process reversely to make sure the ending point is inside the window. The results will eventually show how the amplification factor and position parameter evolve.

In order to distinguish different orbits only from the amplification factor, we have tried two different methods, one is the time-average method, and the other is the low ω method. In the time-average method, we separate the time into several groups and use the average value in each group to see the difference. However, due to the high oscillation behavior when ω is much larger than 1, the amplification factor will be very sensitive to sample numbers and frequency. Whether being able to distinguish peak magnification position will also be affected by the inner orbital types. In the low ω method, we only concentrate on the low ω region, in which the amplification factor hasn't shown great oscillation but already had the first few peaks. A parameter combination should be chosen to satisfy both the ω region and the time ratio conditions. One example we chose has shown the obvious difference for different incoming directions. The incoming direction is represented by the velocity angle between $[0, 0.5\pi]$, inside this region smaller angle will lead to a larger difference between circular and straight outer orbit.

Regarding future work, the improvement could be made in the following parts: the eccentric orbits, high velocity in relativistic cases, retro-lensing, and other environmental influences. The eccentric case will be much more complex because not only the GW from inner BBH will no longer be a single value at the same time, instead a series of harmonics, but also it will lead to a much more complex moving type inside the window.

BIBLIOGRAPHY

Abbott, Benjamin P et al. (2016). “Observation of gravitational waves from a binary black hole merger”. In: *Physical review letters* 116.6, p. 061102.

Amaro-Seoane, Pau and Xian Chen (2016). “Relativistic mergers of black hole binaries have large, similar masses, low spins and are circular”. In: *Monthly Notices of the Royal Astronomical Society* 458.3, pp. 3075–3082.

Bailes, Matthew et al. (2021). “Gravitational-wave physics and astronomy in the 2020s and 2030s”. In: *Nature Reviews Physics* 3.5, pp. 344–366.

D’Orazio, Daniel J and Abraham Loeb (2020). “Repeated gravitational lensing of gravitational waves in hierarchical black hole triples”. In: *Physical Review D* 101.8, p. 083031.

Heggie, Douglas C (1975). “Binary evolution in stellar dynamics”. In: *Monthly Notices of the Royal Astronomical Society* 173.3, pp. 729–787.

Nakamura, Takahiro T (1998). “Gravitational lensing of gravitational waves from inspiraling binaries by a point mass lens”. In: *Physical review letters* 80.6, p. 1138.

Peters, Philip C and Jon Mathews (1963). “Gravitational radiation from point masses in a Keplerian orbit”. In: *Physical Review* 131.1, p. 435.

Peters, Philip Carl (1964). “Gravitational radiation and the motion of two point masses”. In: *Physical Review* 136.4B, B1224.

Rodriguez, Carl L, Pau Amaro-Seoane, et al. (2018). “Post-Newtonian dynamics in dense star clusters: Formation, masses, and merger rates of highly-eccentric black hole binaries”. In: *Physical Review D* 98.12, p. 123005.

Rodriguez, Carl L, Sourav Chatterjee, and Frederic A Rasio (2016). “Binary black hole mergers from globular clusters: Masses, merger rates, and the impact of stellar evolution”. In: *Physical Review D* 93.8, p. 084029.

Samsing, Johan, Morgan MacLeod, and Enrico Ramirez-Ruiz (2014). “The formation of eccentric compact binary inspirals and the role of gravitational wave emission in binary–single stellar encounters”. In: *The Astrophysical Journal* 784.1, p. 71.

Schmidt, Patricia (2020). “Gravitational waves from binary black hole mergers: Modeling and observations”. In: *Frontiers in Astronomy and Space Sciences* 7, p. 28.

Takahashi, Ryuichi and Takashi Nakamura (2003). “Wave effects in the gravitational lensing of gravitational waves from chirping binaries”. In: *The Astrophysical Journal* 595.2, p. 1039.

Wambsganss, Joachim (1998). “Gravitational lensing in astronomy”. In: *Living Reviews in Relativity* 1, pp. 1–74.

Wen, Linqing (2003). “On the eccentricity distribution of coalescing black hole binaries driven by the Kozai mechanism in globular clusters”. In: *The Astrophysical Journal* 598.1, p. 419.

Yu, Hang et al. (2021). “Detecting gravitational lensing in hierarchical triples in galactic nuclei with space-borne gravitational-wave observatories”. In: *Physical Review D* 104.10, p. 103011.